Amplitude breathers in conjugated polymers

S. R. Phillpot
Materials Science Division, Argonne National Laboratory, Argonne, Illinois 60439

A. R. Bishop
Theoretical Division and Center for Nonlinear Studies, Los Alamos National Laboratory, Los Alamos, New Mexico 87545

B. Horovitz
Department of Physics, Ben-Gurion University, P.O. Box 653, 84 105 Beer-Sheva, Israel
(Received 27 June 1988)

Nonlinear adiabatic dynamics of electron-phonon models of *trans*-$(CH)_x$, *cis*-$(CH)_x$, and $(AB)_x$-type polymers are studied. Using both analytic low-amplitude expansion and numerical simulations, we find the existence of charge-neutral breathers—spatially localized, time-periodic nonlinear excitations. Simulations also show that a photoexcited electron-hole pair generates a breather in addition to a soliton-antisoliton pair. Semiclassical quantization shows that the nth breather is a bound state of n amplitude phonons. A semiclassical formalism of optical absorption is applied to *trans*-$(CH)_x$; the ground-state result accounts for a pronounced intragap absorption tail, while breathers can account for the observed photoinduced absorption at 1.35 eV.

I. INTRODUCTION

There has been considerable interest over the last decade in nonlinear excitation of conjugated polymers[1] such as polyacetylene, $(CH)_x$. Most theoretical studies have focused on configurations where the ions are static, e.g., kink solitons, polarons, and bipolarons. In particular, the kink solution in *trans*-$(CH)_x$ is a topologically nontrivial object;[2–5] and in this sense it is similar to solitons in one-dimensional scalar field theories with degenerate minima,[6] e.g., the sine-Gordon or ϕ^4 systems.

Allowing for ion dynamics is an obvious extension of the above studies. The study of dynamics has a twofold motivation. First, it is known that the sine-Gordon system has breather solutions[6] which depend nontrivially on time. A breather is an intrinsically dynamic bound state, representing a spatially localized, time-periodic nonlinear excitation. Numerical studies on the ϕ^4 system,[7,8] have shown the presence of breatherlike states which persist over extremely long times. A recent study of the ϕ^4 system has shown[9] that, while breathers are exact solutions in any order in perturbation theory, a weak essential singularity eventually causes these breathers to decay.

Our second motivation is photoinduced absorption (PA) studies in conjugated polymers. Adiabatic dynamic simulations of *trans*-$(CH)_x$ have shown[10,11] that an initial electron-hole pair decays into a pair of charged solitons. This prediction is supported by PA data[12] which shows a soliton "midgap" absorption at ~ 0.5 eV and three associated infrared lines below ~ 0.15 eV. The PA data show, however, a third feature,[12–15] viz., a peak at 1.35 eV which is just below the absorption gap of ~ 1.7 eV. This so-called "high-energy" (HE) peak is a signature of an additional neutral excitation (with no associated infrared activity) and its temperature and dependence on exciting laser intensity are distinct from those of the midgap absorption.

trans-$(CH)_x$ is a unique polymer type since it has two degenerate ground states [Fig. 1(a)]; a topological solution is then allowed. This degeneracy survives in the $(AB)_x$-type polymer[16] [Fig. 1(c)] but is absent in *cis*-$(CH)_x$ [Fig. 1(b)]. *cis*-$(CH)_x$ represents a more-typical conjugated polymer where the soliton-type "midgap" PA is absent. The HE feature, however, persists in a variety of polymers such as *cis*-$(CH)_x$,[13,16] polydiacetylenes,[16] and poly(1,6-heptadiyne).[17] The HE feature persists also

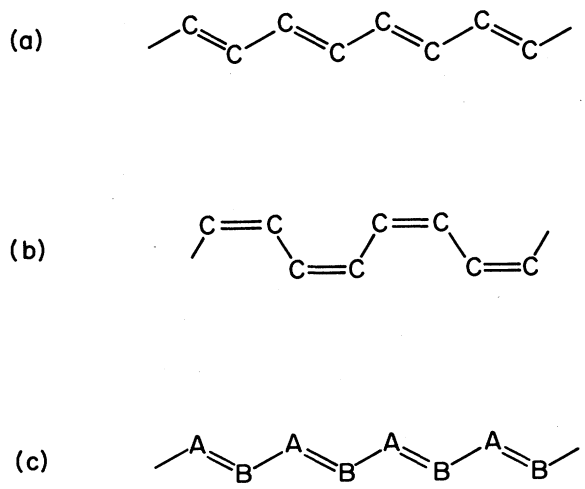

FIG. 1. Dimerization configurations of (a) *trans*-$(CH)_x$ chain, (b) *cis*-$(CH)_x$ chain, (c) $(AB)_x$ chain. Additional H atoms in (a) and (b) and other possible side groups in (c) are not shown. Double and single lines are short and long bonds, respectively.

in doped *trans*-$(CH)_x$ (Ref. 18) and in *trans-cis* $(CH)_x$ mixtures.[19]

In the present work we extend our previous study of breathers in conjugated polymers[20,21] by exploring the adiabatic dynamics of the Su-Schrieffer-Heeger[2] (SSH) electron-phonon model of *trans*-$(CH)_x$ and its extensions to describe *cis*-$(CH)_x$ (Ref. 22) and $(AB)_x$-type polymers.[22,23] The latter corresponds to poly-(1,6-heptadiyne) and to organic mixed stack systems.[24] We show that breathers can account the HE peak in PA experiments. Furthermore, we find that our results also show a pronounced tail of the ground-state absorption into the adiabatic gap, as is indeed seen in experimental data.[25–27]

In Sec. II we start from the continuum version of the SSH Hamiltonian. Using a low amplitude expansion we find analytic breather solutions for the three cases of Fig. 1. A reader who is mainly interested in experimental implications may skip this section and proceed directly to Sec. III. In Sec. III we confirm the existence of breather solutions with numerical adiabatic dynamics[10] of the SSH-type models for *trans*- and *cis*-$(CH)_x$; $(AB)_x$ polymers have breathers only if the difference in *A-B* potentials is not too large. We show that the breathers found numerically are well approximated by the analytic form. The numerical scheme is also applied to photoexcited electron-hole pairs and shows that in *trans*-$(CH)_x$ and in $(AB)_x$ polymers a soliton pair and a breather are generated. In Sec. IV we apply semiclassical quantization to the analytic solutions and find that breathers have a discrete spectrum—the nth breather corresponds to a bound state of n phonons. The binding energy vanishes in the $(AB)_x$ polymer if the difference in *A-B* potentials is too large; this may correspond to the numerical instability of Sec. III.

A significant signature of a breather is its unusual optical absorption, which we study in Sec. V using a semiclassical formalism.[28] We find that breathers can account for the observed PA in conjugated polymers.[12–19] In Sec. VI we compare our results with experimental data and propose additional experiments. The appendixes derive the current operator and the optical sum rule.

II. ANALYTIC BREATHERS

We start here from a continuum description of a one-dimensional electron-phonon system with one electron per site. This can be derived from the SSH model[5] or from other discrete models. In *trans*-$(CH)_x$ [Fig. 1(a)], a spontaneous dimerization appears and yields a gap $2\Delta_0$ at the Fermi level. Competing gaps can results from the *cis* structure [Fig. 1(b)] or the $(AB)_x$ structure [Fig. 1(c)]. The continuum description is valid if $a \ll v_F/\Delta_0$ where v_F is the Fermi velocity (in the absence of a gap) and a is the lattice constant. We also assume the adiabatic limit below, i.e., the bare phonon frequency ω_0 satisfies $\omega_0 \ll \Delta_0$.

A. *trans*- and *cis*-$(CH)_x$

We consider first the case of *trans*- and *cis*-$(CH)_x$. Even in the absence of any dimerization *cis*-$(CH)_x$ has an extrinsic gap $2\Delta_e$ at the Fermi surface.[23] The electron-phonon coupling lead to dimerization with an intrinsic gap $2\Delta_i$, i.e., the total gap is $2\Delta_e+2\Delta_i$. We allow for a space- and time-dependent $\Delta_i(x,t)=4\beta\tilde{u}(x,t)$, where $u_n(t)$ is the ion displacement at site n, $\tilde{u}(x=na,t)=(-1)^n u_n(t)$ is the slowly varying staggered displacement, and β is the electron-phonon coupling constant. Note that Δ_e is both space and time independent.

The electrons are described by a spinor $\psi_s^\dagger(x)=(u_s^*(x),v_s^*(x))$, where $u_s(x),v_s(x)$ are right- and left-moving fields with velocities $\pm v_F$, respectively, and s is a spin index. The electrons respond to the total gap function $\Delta(x,t)=\Delta_i(x,t)+\Delta_e$; the ubiquitous *trans*-$(CH)_x$ case corresponds to $\Delta_e=0$.

The continuum model Hamiltonian is[5,22]

$$\mathcal{H}=\sum_s \int dx\, \psi_s^\dagger(x)\left[-iv_F\sigma_3\frac{\partial}{\partial x}+\Delta(x,t)\sigma_1\right]\psi_s(x) + \int dx \frac{1}{2\pi\lambda v_F}\left[\Delta_i^2(x,t)+\frac{\dot{\Delta}_i^2(x,t)}{\omega_0^2}\right], \tag{1}$$

where the canonical momentum of Δ_i is $\dot{\Delta}_i/(\pi\lambda v_F\omega_0^2)$; σ_1,σ_3 are Pauli matrices, ω_0 is the bare phonon frequency, and $\lambda\sim\beta^2$ is a dimensionless electron-phonon coupling constant [see below, Eq. (23)]. The ground state has a constant $\Delta(x,t)=\Delta_0$, the electron spectrum is $\pm(v_F^2k^2+\Delta_0^2)^{1/2}$ with the momentum k in the range $-E_c/v_F<k<E_c/v_F$, and $\Delta_0=\Delta_e+2\lambda\Delta_0\ln(2E_c/\Delta_0)$; E_c/v_F defines a momentum cutoff representing the discrete lattice.

For a general slowly varying $\Delta(x,t)$ it is possible to find an effective Lagrangian in terms of $\Delta(x,t)$ and its derivatives.[29] Using a derivative expansion, the electrons' Greens function is first found in terms of $\Delta(x,t)$ and its derivatives. The equation of motion connecting $\Delta(x,t)$ and the electrons is then written in terms of $\Delta(x,t)$, i.e., the electron fields are integrated out. Finally, an effective Lagrangian is found such that the Euler-Lagrange equation of motion for $\Delta(x,t)$ recovers the same equation.

This procedure was carried out in detail[29] for the case of a charge density wave with a complex order parameter $\Delta(x,t)\exp[i\phi(x,t)]$. Our dimerization problem corresponds to a real order parameter.[5] We can therefore take over the previous result provided that only $\Delta(x,t)$ is a field (ϕ is fixed) and that we change[5] $\lambda\to 2\lambda$. The effective Lagrangian to second order in derivatives is then

$$\mathcal{L}=\frac{2}{\pi v_F}\left\{\tfrac{1}{2}\Delta^2\left[\ln\left[\frac{2E_c}{\Delta}\right]+\frac{1}{2}\right]-\frac{\Delta^2}{4\lambda} - \frac{v_F^2\Delta'^2-\dot{\Delta}^2}{24\Delta^2}+\frac{\dot{\Delta}^2}{4\lambda\omega_0^2}+\frac{\Delta\Delta_e}{2\lambda}\right\}, \tag{2}$$

where $\Delta=\Delta(x,t)$, dot is $\partial/\partial t$, and prime is $\partial/\partial x$.

We next expand in powers of $\delta(x,t)$ where $\Delta(x,t)=\Delta_0[1+\delta(x,t)]$. The result to order δ^4 is

$$\mathcal{L}_0=-(2\Delta_0^2/\pi v_F)[-\tfrac{1}{2}\eta+\tfrac{1}{2}\eta\delta^2+\tfrac{1}{6}\delta^3-\tfrac{1}{24}\delta^4 +\tfrac{1}{2}(\partial\delta/\partial\tilde{x})^2-\tfrac{1}{2}\eta(\partial\delta/\partial\tilde{t})^2], \tag{3}$$

where $\eta=1+\Delta_e/(2\lambda\Delta_0)$, $\tilde{x}=x\Delta_0\sqrt{12}/v_F$, $\tilde{t}=t\omega_0\times(2\lambda\eta)^{1/2}$, and $\omega_0\ll\Delta_0$ is assumed. The nonlinear equation of motion is

$$\eta\frac{\partial^2\delta}{\partial\tilde{t}^2}-\frac{\partial^2\delta}{\partial\tilde{x}^2}+\eta\delta+\tfrac{1}{2}\delta^2-\tfrac{1}{6}\delta^3=0\ . \tag{4}$$

The linear terms (phonons) are solved by $\delta\sim\exp(i\omega\tilde{t}-iq\tilde{x})$ with $\omega=(1+q^2/\eta)^{1/2}$. We expect the nonlinear terms to bind a localized solution, i.e., an imaginary $q=i\varepsilon$ and $\omega=1-(1/2\eta)\varepsilon^2<1$ for small ε. This motivates a multiple-scale perturbation expansion such that

$$T=\varepsilon^2\tilde{t},\quad X=\varepsilon\tilde{x} \tag{5}$$

and to order ε^3

$$\delta(\tilde{x},\tilde{t})=\varepsilon[A(X,T)e^{i\tilde{t}}+\text{c.c.}]+\varepsilon^2\delta_1(\tilde{x},\tilde{t})+\varepsilon^3\delta_2(\tilde{x},\tilde{t})\ . \tag{6}$$

Note that this expansion is consistent with the order in the derivative expansion of Eq. (2). The $\partial^2\delta/\partial\tilde{t}^2$ term in Eq. (4) is of order ε^3 and higher-order derivatives will not affect the order ε^3 result. [As shown below, δ_1 depends on $\tilde{x}$ through $A(X,T)$; hence $\partial^2\delta_1/\partial\tilde{t}^2=O(\varepsilon^2)$.]

After substituting Eq. (6) in (4) we choose δ_1 so that the $O(\varepsilon^2)$ terms cancel with the result

$$\delta_1(\tilde{x},\tilde{t})=\frac{1}{6\eta}(A^2e^{2i\tilde{t}}+\text{c.c.})-\frac{1}{\eta}|A|^2\ . \tag{7}$$

We then choose δ_2 so that the harmonics $\exp(\pm3i\tilde{t})$ cancel:

$$\delta_2(\tilde{x},\tilde{t})=\frac{1-\eta}{48\eta^2}A^3e^{3i\tilde{t}}+\text{c.c.} \tag{8}$$

Finally, the coefficient of $\exp(\pm i\tilde{t})$ satisfies

$$2i\eta\frac{\partial A}{\partial t}-\frac{\partial^2A}{\partial X^2}-\frac{5+3\eta}{6\eta}|A|^2A=0\ . \tag{9}$$

This is the nonlinear (cubic) Schrödinger equation which has a well-known soliton solution depending on the sign of the cubic term.[6] In particular, for the negative sign in Eq. (9) the soliton is

$$A=\alpha\,\text{sech}(\tilde{\varepsilon}\tilde{x})\exp(-i\tilde{\varepsilon}^2\tilde{t}/2\eta)\ , \tag{10}$$

where $\tilde{\varepsilon}=\varepsilon\alpha[(5+3\eta)/12\eta]^{1/2}$ and α is arbitrary. Combining all the terms we find

$$\delta(\tilde{x},\tilde{t})=\tilde{\varepsilon}\left[\frac{48\eta}{5+3\eta}\right]^{1/2}\text{sech}(\tilde{\varepsilon}\tilde{x})\cos\left[\left[1-\frac{1}{2\eta}\tilde{\varepsilon}^2\right]\tilde{t}\right]+\tilde{\varepsilon}^2\left[\frac{12}{5+3\eta}\right]\text{sech}^2(\tilde{\varepsilon}\tilde{x})\times\left\{\tfrac{1}{3}\cos\left[2\left[1-\frac{1}{2\eta}\tilde{\varepsilon}^2\right]\tilde{t}\right]-1\right\}\ . \tag{11}$$

Solution (11) represents a breather, i.e., a spatially localized, time-periodic nonlinear excitation. The oscillations have frequency $\omega=1-\frac{1}{2}\tilde{\varepsilon}^2$, less than 1, as expected. It is a valid solution if $(5+3\eta)/\eta>0$; this range included *trans*-$(CH)_x$ ($\eta=1$) and excitations around the ground state of *cis*-$(CH)_x$ ($\eta>1$).

Note that *cis*-$(CH)_x$ also has a metastable minimum where the single and double bonds of Fig. 1(b) are interchanged. The gap $\bar{\Delta}_0$ of the metastable state satisfies $\bar{\Delta}_0=-\Delta_e+2\lambda\bar{\Delta}_0\ln(2E_c/\bar{\Delta}_0)$, and $\bar{\Delta}_0=\Delta_i-\Delta_e$. Solution (11) is a valid excitation of the metastable phase with $\eta=1-\Delta_e/(2\lambda\bar{\Delta}_0)<1$. The metastable state is a local minimum only if $\eta>0$ [note the $\eta\delta^2$ term in Eq. (3)]; $\eta>0$ precisely allows the breather solution Eq. (11).

We term solution (11) an "amplitude breather" since it describes localized oscillations in a charge-density-wave amplitude. Charge density waves with commensurability order higher than 2 have a complex order parameter with phase variations requiring much less energy than amplitude variations. The equation for the phase field is the familiar sine-Gordon equation[29] and its breathers might be called "phase breathers."

Consider next the breather *energy*. The Hamiltonian is obtained from Eq. (3) and substituting δ and $\dot{\delta}$ from Eq. (11) at any convenient time t yields for the breather energy

$$E_B(\tilde{\varepsilon})=\Delta_0\frac{\eta^2 16\sqrt{3}}{\pi(5+3\eta)}\tilde{\varepsilon}\left[1-\left[1-\frac{32}{9\eta(5+3\eta)}\right]\frac{\tilde{\varepsilon}^2}{\eta}\right]\ . \tag{12}$$

For the *trans*-$(CH)_x$ case ($\eta=1$),

$$E_B(\tilde{\varepsilon})=\Delta_0\frac{2\sqrt{3}}{\pi}\tilde{\varepsilon}(1-\tfrac{5}{9}\tilde{\varepsilon}^2)\ . \tag{13}$$

Recall that $\tilde{\varepsilon}$ is a continuous parameter and that our expansion is valid for $\tilde{\varepsilon}\ll1$. By analogy with the solvable sine-Gordon system[6] we expect that $E_B(\tilde{\varepsilon})$ is a monotonic function and that breathers exist up to some critical $\tilde{\varepsilon}_c$ of order 1. In *trans*-$(CH)_x$ the breather can unbind into two solitons each with energy $2\Delta_0/\pi$,[2-5] i.e., $E_B(\tilde{\varepsilon}_c)=4\Delta_0/\pi$. Note that $\tilde{\varepsilon}_c$ cannot be deduced from Eq. (13), which is based on a small $\tilde{\varepsilon}$ expansion.

B. $(AB)_x$ polymers

Consider Fig. 1(c) where a *trans*-$(CH)_x$-type chain is allowed to have an alternating on-site potential $(-1)^n\alpha$. For 1 electron per site (in the absence of dimerization) this yields a gap 2α at the Fermi level. Spontaneous dimerization is possible if $\alpha<\Delta_0$, where $2\Delta_0$ is the gap for $\alpha=0$. Unlike *cis*-$(CH)_x$, dimerization here is symmetry breaking (that of inversion symmetry[24]) and yields degenerate bound states, thus allowing topological solitons.[23]

The continuum model for an $(AB)_x$ polymer is[5,22-24]

$$\mathcal{H}=\sum_s\int dx\,\psi_s^\dagger(x)\left[-iv_F\sigma_3\frac{\partial}{\partial x}+\Delta_d(x,t)\sigma_1+\alpha\sigma_2\right]\psi(x)+\int dx\frac{1}{2\pi\lambda v_F}[\Delta_d^2(x,t)+\dot{\Delta}_d^2(x,t)/\omega_0^2]\ . \tag{14}$$

The off-diagonal terms in (14) imply a complex gap function

$$\Delta(x,t)\exp[i\phi(x,t)]=\Delta_d(x,t)+i\alpha\ . \tag{15}$$

Thus α, which corresponds to a site-centered density wave, is out of phase with Δ_d, which describes a bond-centered density wave. [Compare with *cis*-$(CH)_x$ where both Δ_i, Δ_e are bond density waves and $\Delta=\Delta_i+\Delta_e$ is additive.]

Since the amplitude $\Delta(x,t)$ and phase $\phi(x,t)$ in (15) are constrained by $\Delta(x,t)\sin\phi(x,t)=\alpha$, the effective Lagrangian must be rederived. Using Eq. (A17) of Ref. 26 we obtain

$$\Delta_d+\ddot{\Delta}_d/\omega_0^2=2\lambda\{\Delta\cos\phi\ln(2E_c/\Delta) -(4\Delta)^{-1}(v_F^2\phi''-\ddot{\phi})\sin\phi -(12\Delta^3)^{-1}[v_F^2(\Delta')^2-\dot{\Delta}^2-v_F^2\Delta\Delta'' +\Delta\ddot{\Delta}]\cos\phi\} . \quad (16)$$

Rewriting this in terms of $\Delta_d(x,t)$ and its derivatives yields an equation which is the variational Euler-Lagrange equation of the Lagrangian

$$\mathcal{L}\{\Delta_d\}=\frac{2}{\pi v_F}\left\{\tfrac{1}{2}\Delta^2\left[\ln\left[\frac{2E_c}{\Delta}\right]+\frac{1}{2}\right]-\frac{\Delta_d^2}{4\lambda}+\frac{\dot{\Delta}_d^2}{4\lambda\omega_0^2} -\frac{3\alpha^2+\Delta_d^2}{24\Delta^4}[v_F^2(\Delta_d'^2)-\dot{\Delta}_d^2]\right\} . \quad (17)$$

The ground state has $\Delta_d=\Delta_d^0$, where

$$[(\Delta_d^0)^2+\alpha^2]^{1/2}=\Delta_0\equiv 2E_c\exp(-1/2\lambda) . \quad (18)$$

Clearly $\Delta_d^0\neq 0$ only if $\alpha<\Delta_0$. We next expand (17) around the minimum $\Delta_d(x,t)=\Delta_d^0[1+\delta(x,t)/(3-2\gamma)]$, where $\gamma=(\Delta_d^0/\Delta_0)^2<1$. To order δ^4 we obtain

$$\mathcal{L}=-\frac{2\Delta_0^2\gamma^2}{\pi v_F(3-2\gamma)^2}\left[\tfrac{1}{2}\delta^2+\tfrac{1}{6}\delta^3-\frac{12\gamma-3-8\gamma^2}{24(3-2\gamma)^2}\delta^4 +\frac{1}{2}\left[\frac{\partial\delta}{\partial\bar{x}}\right]^2-\frac{1}{2}\left[\frac{\partial\delta}{\partial\bar{t}}\right]^2\right] . \quad (19)$$

where $\bar{x}=[12\gamma/(3-2\gamma)]^{1/2}x\Delta_0/v_F$, $\bar{t}=t\omega_0(2\lambda\gamma)^{1/2}$, and $\omega_0\ll\Delta_0$ is assumed. Using the expansion (6) with $\bar{x},\bar{t}$ replacing $\bar{x},\bar{t}$ we obtain the nonlinear Schrödinger equation

$$2i\frac{\partial A}{\partial T}-\frac{\partial^2 A}{\partial X^2}-\frac{2(9-6\gamma-\gamma^2)}{3(3-2\gamma)^2}|A|^2A=0 . \quad (20)$$

For the relevant range $0<\gamma<1$ the cubic term has a negative coefficient and amplitude breathers exist. The breather solution is

$$\delta(\bar{x},\bar{t})=\bar{\varepsilon}(3-\gamma)[12/(9-6\gamma-\gamma^2)]^{1/2} \times\operatorname{sech}(\bar{\varepsilon}\bar{x})\cos[(1-\tfrac{1}{2}\bar{\varepsilon}^2)\bar{t}] +\bar{\varepsilon}^2 3(3-2\gamma)^2(9-6\gamma-\gamma^2)^{-1}\operatorname{sech}^2(\bar{\varepsilon}\bar{x}) \times\{\tfrac{1}{3}\cos[2(1-\tfrac{1}{2}\bar{\varepsilon}^2)\bar{t}]-1\} , \quad (21)$$

where $\bar{\varepsilon}$ (proportional to ε) is a continuous parameter.

The breather energy is obtained by substituting (21) in the Hamiltonian which corresponds to (19), with the result

$$E_B(\bar{\varepsilon})=\Delta_0\frac{4\sqrt{3}\gamma^{3/2}(3-2\gamma)^{1/2}}{9-6\gamma-\gamma^2} \times\bar{\varepsilon}\left[1-\left[1-\frac{8(3-2\gamma)^2}{9(9-6\gamma-\gamma^2)}\right]\bar{\varepsilon}^2\right] . \quad (22)$$

For $\gamma=1$ this reproduces the *trans*-$(CH)_x$ result, Eq. (13).

III. NUMERICAL BREATHERS

In this section we study breathers by numerical simulations. We show that breathers can be produced by a photoexcited electron-hole pair, and then compare them with breathers generated by the analytic solution of Sec. II.

Consider the SSH Hamiltonian[2] on a *trans*-$(CH)_x$ chain, with $C_{n,s}^\dagger$ creating an electron with spin s at site n and u_n the nth-ion displacement:

$$\mathcal{H}=-\sum_{n,s}[t_0+\beta(u_n-u_{n+1})][C_{n+1,s}^\dagger C_{n,s}+\text{H.c.}] +\tfrac{1}{2}K\sum_n(u_{n+1}-u_n)^2+\tfrac{1}{2}M\sum_n\dot{u}_n^2 . \quad (23)$$

Here, t_0 is the transfer integral, β the electron-phonon coupling, K the ion spring constant, and M the ion mass. The continuum version Eq. (1) is identified by[5] $\lambda=2\beta^2/(\pi t_0 K)$, $v_F=2t_0a$, and the bare-phonon frequency at wave vector π/a, $\omega_0=2(K/M)^{1/2}$.

The adiabatic dynamics simulations[10,30] are obtained by a loop of two steps. First solve the electron eigenvectors $\hat{f}_{\alpha,s}=\sum_n f_\alpha(n)C_{n,s}$ with eigenvalues ϵ_α as if the lattice $u_n(t)$ is time independent, i.e.,

$$\epsilon_\alpha f_\alpha(n)=-[t_0+\beta(u_n-u_{n+1})]f_\alpha(n+1) -[t_0+\beta(u_{n-1}-u_n)]f_\alpha(n-1) . \quad (24)$$

Second, evolve $u_n(t)$ in time by the classical ion dynamics

$$M\ddot{u}_n=-K(2u_n-u_{n+1}-u_{n-1})-\frac{\partial}{\partial u_n}\sum_{\alpha,s}l_{\alpha,s}\epsilon_\alpha , \quad (25)$$

where $l_{\alpha,s}$ is the occupancy of level α with spin s ($l_{\alpha,s}=0$ or 1) and is time independent. The last term of (25) is the force on the ion due to the interaction term in (25); ϵ_α are functions of the instantaneous $u_n(t)$ via Eq. (24). Integrating Eq. (25) yields a new set of $u_n(t)$ for which Eq. (24) yields new eigenvectors and a new force in (25). This repeated cycle of solving Eqs. (24) and (25) is termed "adiabatic dynamics."

Before considering photoexcitation experiments, it is necessary to briefly review some aspects of the adiabatic dynamics of a single kink. Previously[20] we have numerically shown that for the short-time dynamics of a single boosted kink there is a maximum propagation velocity (v_m), above which uniform kink translation is not observed and an oscillating tail structure develops. (For times longer than one phonon period, phonon effects becomes important, especially in discrete cases, and the dynamics changes somewhat.) We argued that v_m, which can be *greater* than the sound velocity (depending on the coherence length v_F/Δ_0), is determined by the finite response time of the lattice to changes in its dimerization.

A simple ansatz calculation confirmed this and gave an estimate of v_m in qualitative agreement with that observed numerically. This (short-time) maximum velocity corresponds to a maximum kinetic energy of $\sim 0.1\Delta_0$, approximately independent of the parameter values in the SSH Hamiltonian.

The parameters used below correspond to $t_0=2.5$ eV, $\beta=4.8$ eV/Å, $K=17.3$ eV/Å^2. Choosing $M=13$ a.u. gives $\omega_0=2.25\times 10^{14}$ sec^{-1} and the time unit in the plots is one femtosecond. For classical ions energy, length and time can be chosen dimensionless; hence a single parameter $\lambda=2\beta^2/(\pi t_0 K)$ determines the simulation. For the parameters above $\lambda=0.34$, this yields a ground-state adiabatic gap of $2\Delta_0=3.92$ eV, and a kink half-width of $v_F/\Delta_0\simeq 2.7a$.

The ion displacement patterns shown below are $r_n=\frac{1}{4}(-1)^n[2u_n-u_{n+1}-u_{n-1}]$, which is the dimerization pattern in $u_n=(-1)^n r_n+s_n$. The s_n field is slowly varying[20] and represents modulations in the local lattice constant.

We begin our study of breather production by considering a simple photoexcitation experiment in *trans*-polyacetylene. To simulate an infinite system, a large number of sites (98) is used and periodic boundary conditions applied. In the dimerized ground state all 49 states below the gap are doubly occupied and all 49 states above the gap are empty. Starting from a purely dimerized ring at $t=0$, a single electron is photoexcited (i.e., manually moved) from the top of the valence band to the bottom of the conduction band, adding energy $2\Delta_0$ (the full gap energy). All electrons then remain in these levels throughout the experiment, i.e., the system evolves adiabatically.

Figure 2 shows that within one period ($2\pi/\omega_0\simeq 28$ time units) a rapidly separating kink-antikink pair is formed. The kink and antikink each have rest energy $\sim 2\Delta_0/\pi$ and maximum kinetic energy $\sim 0.1\Delta_0$ giving a total energy of $\sim 1.5\Delta_0$ for the two kinks. In Fig. 2 we see that a substantial fraction of the remaining energy, $\sim 0.5\Delta_0$, is localized as a nonlinear, dynamic, lattice excitation—an amplitude breather. By isolating the central 42 atoms of the breather, we have shown numerically that it is long lived, with no appreciable change in frequency or amplitude after 5 psec, i.e., ~ 130 oscillations, although intermittent interferences and refocusing events were observed.

Figure 3 shows the 49th eigenvalue (singly occupied) and the 48th level (doubly occupied) as functions of time. Note that charge conjugation symmetry[2,10] of Eq. (24) implies that for each level at ϵ_α there is a level at $-\epsilon_\alpha$; thus $\epsilon_{50}=-\epsilon_{49}$, $\epsilon_{51}=-\epsilon_{48}$, etc. Figure 3 then shows that the midgap states associated with the kinks rapidly settle to zero. The next state is also split significantly from the continuum states and exhibits large scale oscillations. These states (48 and 51) are the predominant signature of the localized breather.

In Fig. 4 we compare the lattice dynamics of the numerical and analytic breathers. Figure 4(a) shows the evolution of the central 42 atoms of Fig. 2 when they are placed on a 42-site ring. Figure 4(b) shows a 42-site chain whose initial condition is the analytic solution [Eq. (11) with $\eta=1$] with $\bar{\epsilon}=0.61$ while subsequent dynamics follows Eqs. (24) and (25). In both cases the 21 lower levels are doubly occupied while the upper 21 levels are empty.

The choice $\bar{\epsilon}=0.61$ gave the best fit to the *frequency* of the numerical breather. Its energy of $\sim 0.53\Delta_0$ [Eq. (13)] accounts for the energy "missing" in the photoexcitation process. Most of the energy of the numerical breather [Fig. 4(a)] is localized in a similar way to the analytic breather [Fig. 4(b)], though some low amplitude oscillations indicate the formation of additional delocalized phonons. Note that the symmetry of *trans*-$(CH)_x$ allows $r_n\rightarrow -r_n$ and the breather of Fig. 4(b) exists also around $r_n=+1$.

It is interesting to consider photoexcitations from nonuniform structures. Consider, e.g., a single polaron[22,31] with rest energy $\sim 2\sqrt{2}\Delta_0/\pi$ and electronic levels at $\pm\Delta_0/\sqrt{2}$ from midgap. Photoexcitation of an electron from the lower to the upper polaron level adds energy $\sqrt{2}\Delta_0$. Thus the photoexcited state has energy

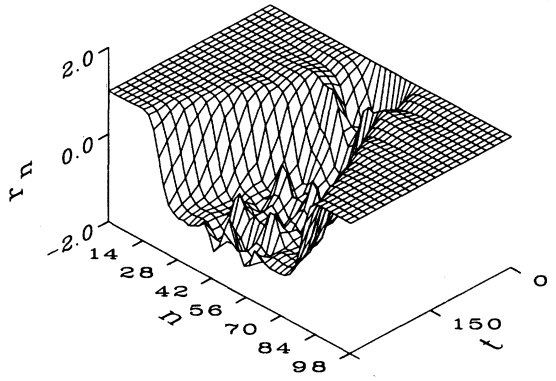

FIG. 2. Time evolution of an excited electron-hole pair in *trans*-$(CH)_x$ with $\lambda=0.34$. This figure shows the dimerization pattern, normalized to that of the ground state, for a 98-site ring with 98 electrons occupying the lowest 48 states by pairs and singly occupying the 49th and 50th states.

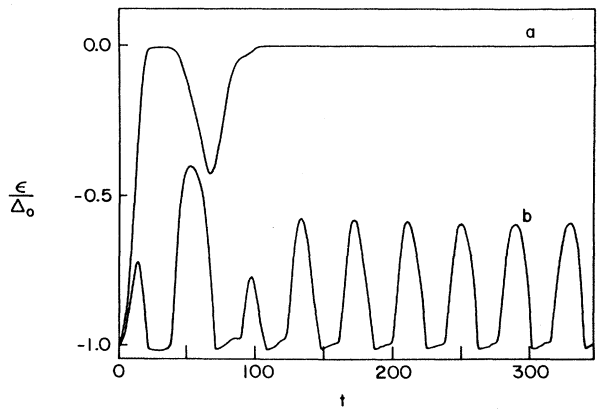

FIG. 3. Time dependence of electron levels corresponding to Fig. 2: (a) the 49th state, rapidly becoming a kink midgap state, (b) the 48th state, which becomes the intragap breather state.

$\sim(2\sqrt{2}/\pi+\sqrt{2})\Delta_0\sim 2.3\Delta_0$ above that of the ground state. Consequently this excited polaron can be expected to be unstable towards formation of a $K\bar{K}$ pair and a breather; the midgap states are now singly and doubly occupied, respectively. Figure 5 shows that indeed a kink pair is rapidly produced together with a large amplitude breather. From energy balance the breather energy is $\sim 0.8\Delta_0$; its amplitude seems too large to be described by the low amplitude expansion of Sec. II.

To study *cis*-$(CH)_x$ we note that even and odd sites in Fig. 1(b) differ by their overlap to the third site along the chain. The Hamiltonian (23) is now supplemented by

$$H_{cis}=t_3\sum_{n\ \text{even}} C^{\dagger}_{n+3}C_n+\text{H.c.} \tag{26}$$

A similar symmetry-breaking term is

$$H'_{cis}=t_1\sum_n(-)^n C^{\dagger}_{n+1}C_n+\text{H.c.} \tag{27}$$

Both Eqs. (26) and (27) reduce to the same Δ_e term in the continuum model with $t_1=\Delta_e$ and $t_3=\frac{1}{3}\Delta_e$, respectively. For slowly varying dimerization patterns, forms (26) and (27) should, therefore, yield similar results.

The presence of the symmetry breaking implies that the bond pattern of Fig. 1(b) is the ground state; unlike *trans*-$(CH)_x$, interchanging the single and double bonds leads to a nondegenerate state which for small Δ_e is metastable. A significant consequence of this nondegeneracy is that isolated topological kinks do not exist—the energy of a kink-antikink pair increases linearly with their separation.

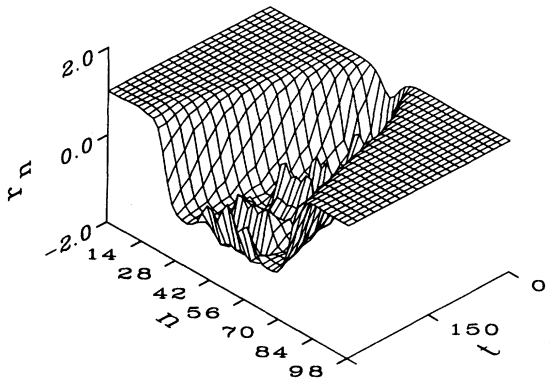

FIG. 5. Time evolution of an excited electron-hole pair from a polaron state in *trans*-$(CH)_x$. The 98-site ring has 99 electrons—the lowest 48 states doubly occupied, the 49th state singly occupied, and the 50th state doubly occupied.

Figure 6 shows the numerical dynamics of an initial electron-hole pair for $H+H'_{cis}$ [Eqs. (23) and (27)]. Figure 6(a) shows a case of weak symmetry breaking, $t_1/t_0=0.002$ (or $\eta=1.0038$) for which the kinks can separate sufficiently to allow the formation of a breather. At longer times the kinks should recombine and interfere with the breather oscillations. Figure 6(b) shows a

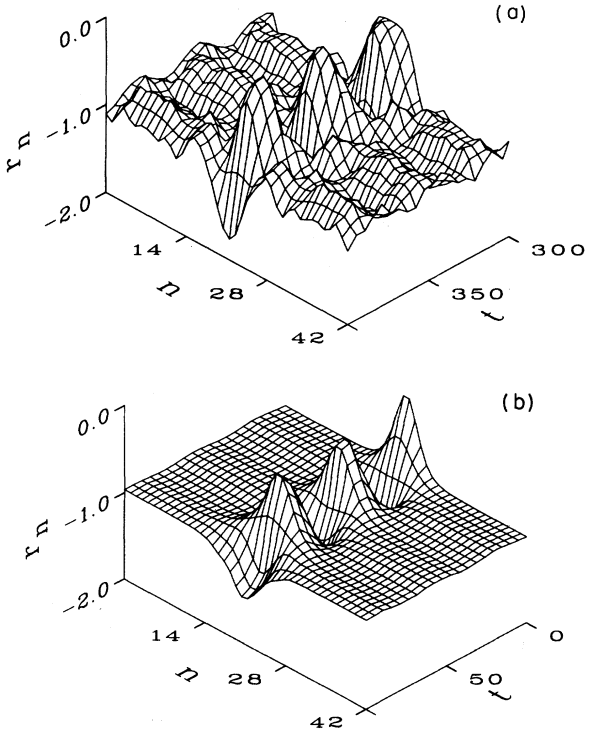

FIG. 4. Dimerization pattern of a 42-site ring with the electrons occupying the lowest 21 states. The initial conditions are (a) the central 42 sites of Fig. 2 at time 300, (b) the analytic form [Eq. (11)] with $\bar{\varepsilon}=0.61$, $\eta=1$.

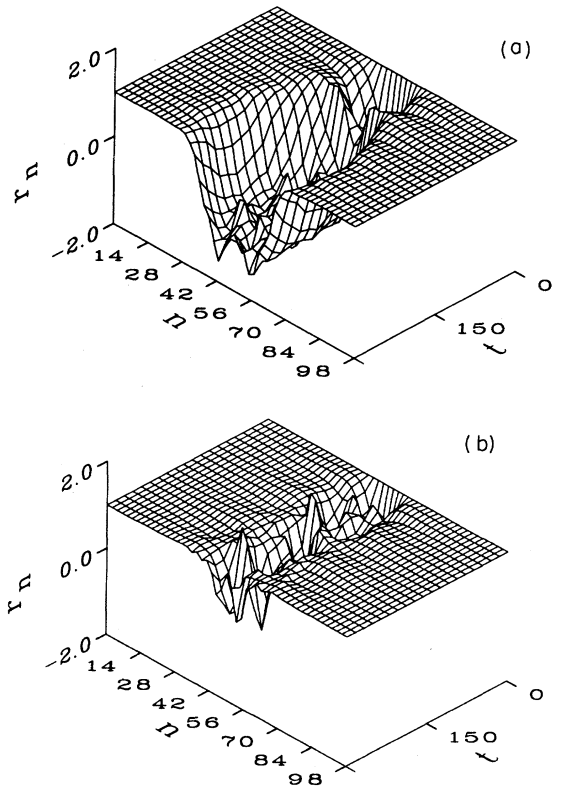

FIG. 6. Same as Fig. 2 for *cis*-$(CH)_x$ with a *cis* parameter of (a) $t_1/t_0=0.002$ ($\eta=1.0038$), (b) $t_1/t_0=0.012$ ($\eta=1.0225$).

stronger symmetry breaking $t_1/t_0=0.012$ (or $\eta=1.0225$) for which separate kinks or a breather cannot be identified. The resulting object is an electron-hole bound state, i.e., an exciton. It is interesting, however, that the exciton levels oscillate periodically and that the kinetic energy remains localized near the exciton. Simulations of other values of t_1 suggest that we can expect dynamical exciton states for a *cis*-$(CH)_x$ structure if $t_1/t_0 \gtrsim 0.015$ (or $\eta \gtrsim 1.03$).

Figure 7 shows numerical simulations starting with the analytic form Eq. (11). For $\bar{\varepsilon}=0.55$ and $t_1=1.0$ (or $\eta=1.75$). In comparing with Fig. 4(b) (where $\bar{\varepsilon}=0.61$ and $t_1=0$) the amplitude is comparable, but the frequency is increased, in agreement with Eq. (11).

Finally, we consider breather states for an $(AB)_x$ polymer [Fig. 1(c)], where the Hamiltonian (23) is supplemented by

$$H_{AB}=\alpha \sum_{n,s} (-1)^n C_{n,s}^{\dagger} C_{n,s} \ . \tag{28}$$

Figure 8 shows the time evolution of a breather with $\alpha/t_0=0.12$ whose initial conditions are the analytic solution Eq. (21), with $\bar{\varepsilon}=0.5$. We find that the breather oscillations are persistent; some acoustic deformation is, generated however, and interferes with the breather as it propagates through the periodic boundaries back to the origin. There is a tendency to form a double maximum, but no further splitting or spreading is observed up to ~ 25 periods.

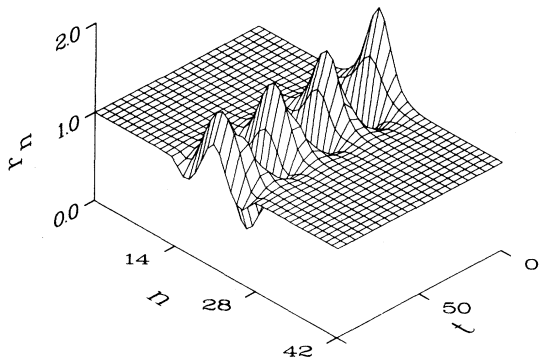

FIG. 7. Dimerization pattern in *cis*-$(CH)_x$ with $\lambda=0.34$ for a breather state. Initial conditions are those of Eq. (11) with $\bar{\varepsilon}=0.55$ and $t_1=1.0$ ($\eta=1.75$).

Figure 9 shows the same evolution for $\alpha/t_0=0.36$. In addition to generating an acoustic deformation, in this case there seems to be an inherent instability by which the number of maxima doubles, i.e., $1\rightarrow 2\rightarrow 4$, and the overall shape spreads with time. The instability is also seen in the irregular oscillations of the intragap level (inset of Fig. 9) and the fast decay of the oscillation amplitude.

Figures 10 and 11 show the dynamics following a photoexcitation. For $\alpha/t_0=0.12$ (or $\alpha/\Delta_0=0.16$) there is sufficient energy to separate the kinks and form a breath-

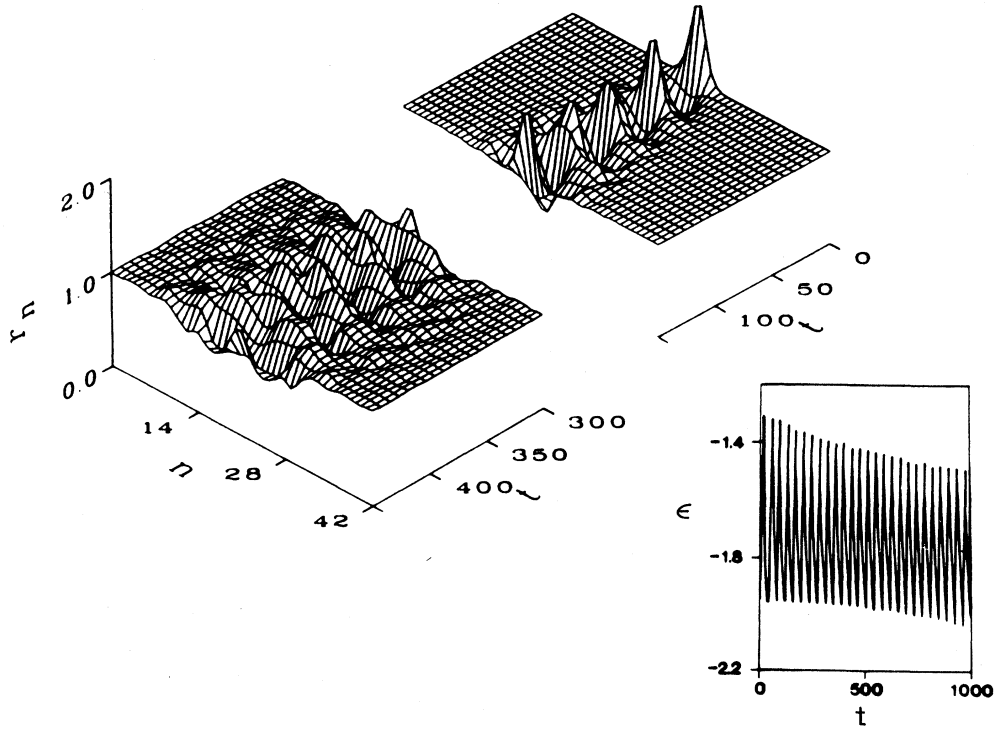

FIG. 8. Dimerization pattern in an $(AB)_x$ polymer with $\lambda=0.34$ and $\alpha/t_0=0.12$ (or $\alpha/\Delta_0=0.15$). The initial condition is a breather [Eq. (21)] with $\bar{\varepsilon}=0.5$. The inset shows the 21st electronic level.

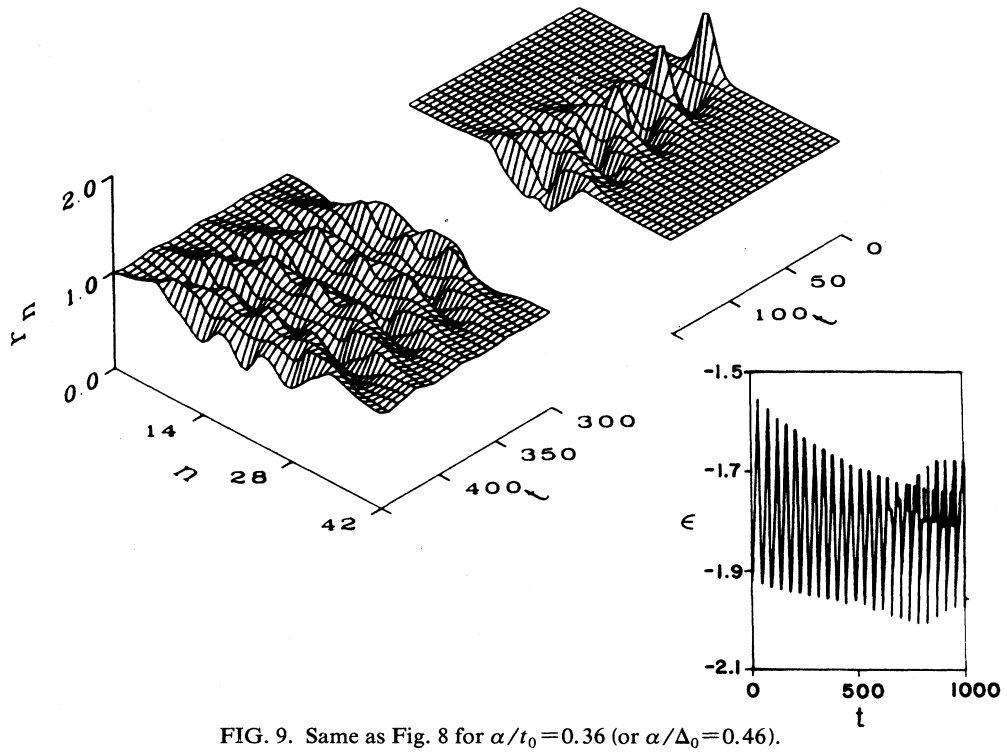

FIG. 9. Same as Fig. 8 for $\alpha/t_0=0.36$ (or $\alpha/\Delta_0=0.46$).

er (Fig. 10). As α increases, the static formation energy of the kink pair[22,23]

$$E_K+E_{\bar{K}}=(4\Delta_0/\pi)[(1-\alpha^2/\Delta_0^2)^{1/2} +(\alpha/\Delta_0)\sin^{-1}(\alpha/\Delta_0)]$$

increases, approaching $2\Delta_0$ as $\alpha\rightarrow\Delta_0$. Figure 11 shows the electron-hole dynamics for $\alpha/t_0=0.24$ (or $\alpha/\Delta_0=0.32$), where one of the generated kinks remains near the center, bound to a localized oscillation.

The insets of Figs. 10 and 11 show the highest occupied levels. The 49th and 50th ($\epsilon_{50}=-\epsilon_{49}$) show the rap-

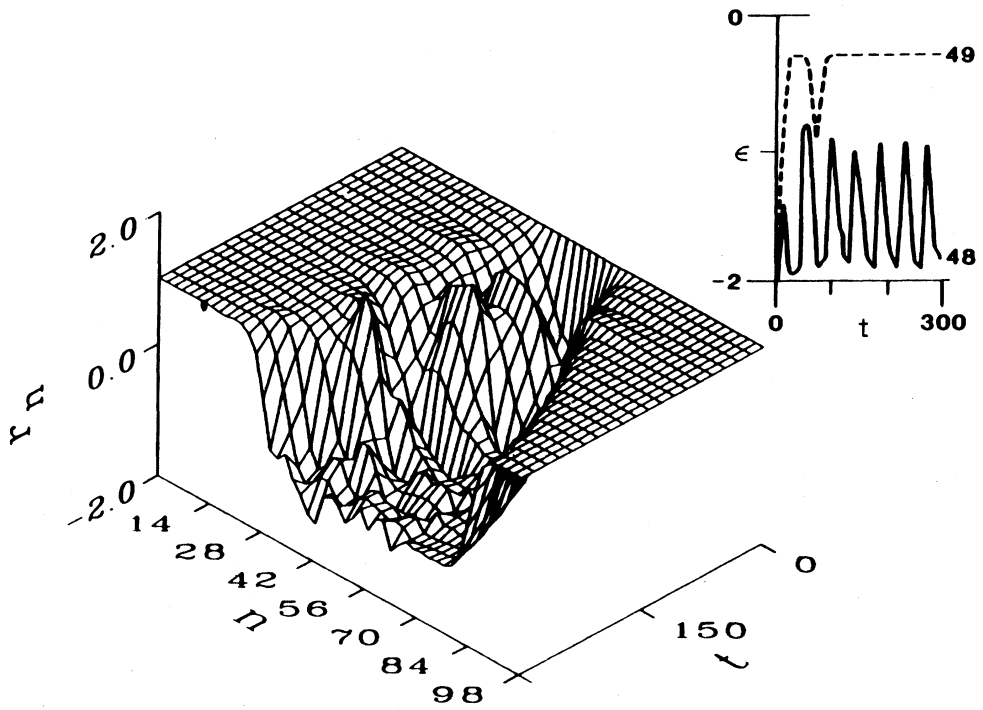

FIG. 10. Time evolution of an excited electron-hole pair in an $(AB)_x$ polymer with $\lambda=0.34$ and $\alpha/t_0=0.12$ (or $\alpha/\Delta_0=0.15$). Level occupancy is as in Fig. 2. The inset shows the 48th and 49th levels.

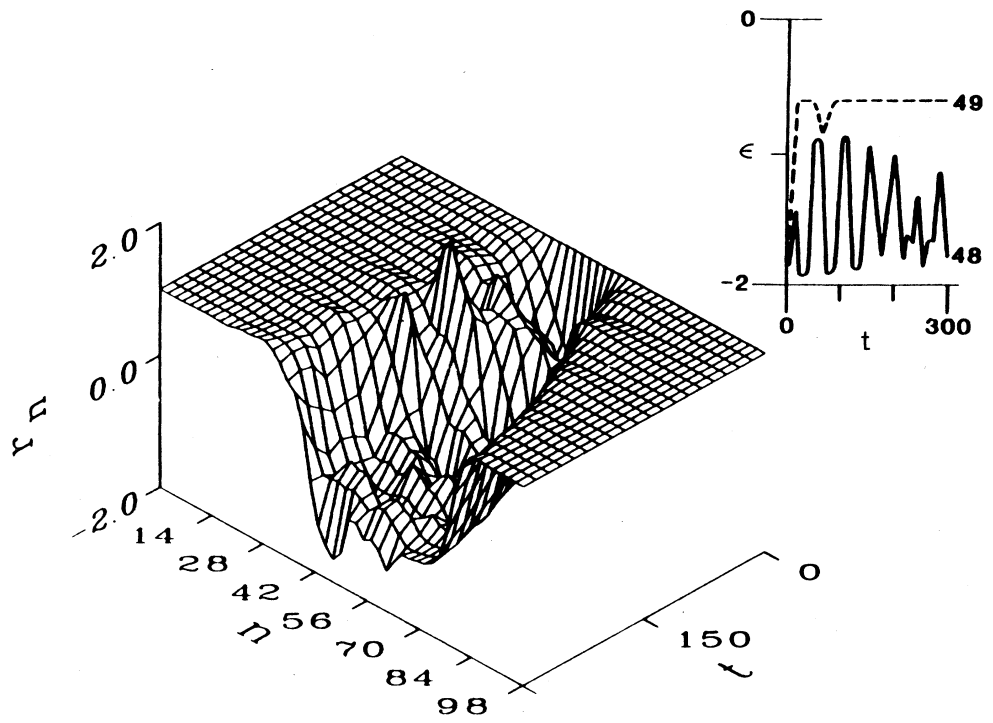

FIG. 11. Same as Fig. 10 for $\alpha/t_0=0.24$ (or $\alpha/\Delta_0=0.31$).

id formation of kink states at $\pm\alpha$. The 48th state, associated with the breather, shows persistent oscillations for $\alpha/t_0=0.12$ which become incoherent for $\alpha/t_0=0.24$.

To conclude this section, we have found that numerical adiabatic dynamics confirms to a large extent the analytic solutions of Sec. II. The dynamic stability of the numerical breathers is affected by a few ingredients. (a) Lattice discreteness which allows the generation of low amplitude acoustic waves. Since our studies are on finite rings, the reentrant effect of these waves limits our ability to study this effect. In general, however, breathers are robust objects and survive collision with acoustic waves as seen in our study of the *trans*-$(CH)_x$ case up to 130 oscillations. (b) There may be nonperturbative corrections to breathers, as in the ϕ^4 theory[9] which limits the breather lifetime even in the continuum model. The acoustic effect is, however, more significant in the numerical study. (c) A new *dynamic* instability appears in the $(AB)_x$ case when $\alpha/\Delta_0 \gtrsim 0.2$. This may be related to an instability in the semiclassical quantization of the analytic solutions, shown in the next section.

IV. QUANTIZED BREATHERS

Periodic classical solutions can be semiclassically quantized[32] by an integer $n \geq 0$ such that

$$2\pi\hbar(n+\tfrac{1}{2})=\int dx \int_0^{2\pi/\omega_B} \Pi(x,t)\dot{\Delta}(x,t)dt \ , \tag{29}$$

where ω_B is the breather frequency, $\Pi(x,t)=\delta\mathcal{L}/\delta\dot{\Delta}$ with $\mathcal{L}$ of Eq. (2), and $\Pi(x,t),\dot{\Delta}(x,t)$ evaluated with the breather solutions, Eq. (11).

Equation (29) yields quantized values to the parameter $\bar{\varepsilon}$ and quantized breather energies. The small expansion parameter becomes $\bar{\varepsilon}\sim\omega_0/\Delta_0$ so that the nonlinear $\bar{\varepsilon}^3$ terms in (13) become nonadiabatic terms. Thus quantization reveals that the expansion in ε is identical to the adiabatic expansion in powers of ω_0/Δ_0.

A minor alteration in the solutions of Sec. II is now needed, taking care of a comparable correction to the kinetic energy. Equation (2) contains an electronic kinetic energy $\sim\dot{\Delta}^2/\Delta^2$ which is small compared with the ion kinetic energy by $\sim(\omega_0/\Delta_0)^2$ and is therefore neglected in the classical adiabatic limit. Since $(\omega_0/\Delta)^2\dot{\Delta}^2=O(\varepsilon^4)$, the highest order used in Sec. II, one can replace Δ by Δ_0 in the electron kinetic term. Considering first the *trans*- and *cis*-$(CH)_x$ model, the linearized equation for $\delta(x,t)$ has then the renormalized frequency

$$\omega_R=\omega_0(2\lambda\eta)^{1/2}(1+\tfrac{1}{6}\lambda\omega_0^2/\Delta_0^2)^{-1/2} \tag{30}$$

and the breather frequency from Eq. (11) is $\omega_B=\omega_R(1-\bar{\varepsilon}^2/2\eta)$. The parameter $\bar{\varepsilon}$ is determined by substituting $\Pi(x,t)=\eta\dot{\Delta}(x,t)/\omega_R^2$ and solution (11) in quantization (29); the result to order $(\omega_R/\Delta_0)^3$ is

$$\bar{\varepsilon}=\pi(n+\tfrac{1}{2})\frac{\hbar\omega_R}{\Delta_0}\frac{5+3\eta}{8\sqrt{3}\eta^2}+\left[\frac{1}{2\eta}-\frac{8}{9\eta(5+3\eta)}\right]\times\left[\pi(n+\tfrac{1}{2})\frac{\hbar\omega_R}{\Delta_0}\frac{5+3\eta}{8\sqrt{3}\eta^2}\right]^3 . \tag{31}$$

Substituting (31) in (12) yields the energy spectrum for quantized breathers

$$E_B'(n)=\hbar\omega_R(n+\tfrac{1}{2})\left[1-\frac{2}{\eta}(9\eta-1)(5+3\eta)\left[\frac{\pi}{96\eta^2}\right]^2\times\left[\frac{\hbar\omega_R}{\Delta_0}\right]^2(n+\tfrac{1}{2})^2\right]. \quad (32)$$

For $\eta=1$, the *trans*-$(CH)_x$ case, this yields

$$E_B'(n)=\hbar\omega_R(n+\tfrac{1}{2})\left[1-\frac{\pi^2}{72}\left[\frac{\hbar\omega_R}{\Delta_0}\right]^2(n+\tfrac{1}{2})^2\right]. \quad (33)$$

Note that $n=0$ is the zero-point energy correction to the ground state. The breather excitation spectrum, relative to the ground state, is then

$$E_B(n)=E_B'(n)-E_B'(0). \quad (34)$$

The leading term in $E_B(n)$ is $n\hbar\omega_R$—the energy of n phonons. A breather can be interpreted as a bound state of n phonons, the next term in $E_B(n)$ being the binding energy. In fact, even a single phonon has now a renormalized energy $E_B(1)$, though practically $E_B(1)\simeq\hbar\omega_R$ with a very small correction. The breather is a stable bound state if it cannot decay into n phonons, i.e., $E_B(n)<nE_B(1)$. This implies that the energy correction in (32) should be negative, i.e., $\eta>1/9$. Thus breathers in *trans*-$(CH)_x$ ($\eta=1$) are stable and those excited from the ground state of *cis*-$(CH)_x$ ($\eta>1$) are also stable. Breathers excited from the metastable state of *cis*-$(CH)_x$ ($0<\eta<1$) have a range $0<\eta<1/9$ of instability; although a classical solution exists in this range, quantization shows that they are unstable.

Quantization of the $(AB)_x$ solutions proceeds along similar lines. In Eq. (29), replace $\dot{\Delta}(x,t)$ with $\dot{\Delta}_d(x,t)$ and $\Pi(x,t)=\delta\mathcal{L}/\delta\dot{\Delta}_d$ with $\mathcal{L}$ of Eq. (17) and $\Pi(x,t),\dot{\Delta}_d(x,t)$ evaluated with the breather solution Eq. (21). The result to order $(\omega_R/\Delta_0)^3$ is

$$\bar{\varepsilon}=\pi(n+\tfrac{1}{2})\frac{\hbar\omega_R}{\Delta_0}\frac{9-6\gamma-\gamma^2}{4\sqrt{3}(3-2\gamma)^{1/2}\gamma^{3/2}}-\left[\frac{1}{2}-\frac{2(3-2\gamma)^2}{9(9-6\gamma-\gamma^2)}\right]\times\left[\pi(n+\tfrac{1}{2})\frac{\hbar\omega_R}{\Delta_0}\frac{9-6\gamma-\gamma^2}{4\sqrt{3}(3-2\gamma)^{1/2}\gamma^{3/2}}\right]^3. \quad (35)$$

Substituting in (22) yields the quantized spectra

$$E_B'(n)=\hbar\omega_R(n+\tfrac{1}{2})\times\left[1-\frac{(9-6\gamma-\gamma^2)(30\gamma-9-19\gamma^2)}{2(3-2\gamma)\gamma^3}\times\left[\frac{\pi}{12}\right]^2\left[\frac{\hbar\omega_R}{\Delta_0}\right]^2(n+\tfrac{1}{2})^2\right] \quad (36)$$

with the excitation spectra given by (34).

Stability against decay into phonons requires a binding energy in (36), i.e., in the physical range of $0<\gamma<1$ we need $30\gamma-9-9\gamma^2>0$ or $\gamma>0.403$. The corresponding critical AB parameters is $\alpha_c=0.75\Delta_0$. For $\alpha>\alpha_c$ quantization shows that the classical solutions are not valid. An intriguing possibility is that this instability corresponds to the classical dynamic instability which was seen in the simulations of Sec. III. The latter appeared at $\alpha\gtrsim 0.3\Delta_0$ showing a decay to phonons and to lower amplitude breathers (Fig. 9).

V. OPTICAL ABSORPTION

A most significant means for observing amplitude breathers is by their optical absorption. The electron "intragap" states localized at the breather allow for transitions below the adiabatic gap. In fact, even the quantized ground state ($n=0$) allows for such transitions. We thus derive here both an absorption tail of the ground state and intragap peaks of breather absorptions.

We have recently developed a semiclassical formalism for deriving the optical absorption in the presence of a time-periodic structure.[28] The formalism assumes the following. (a) The semiclassical condition for the initial state which corresponds here to $\hbar\omega_B\ll 2\Delta_0$. Also the excited state should be separated by more than $\hbar\omega_B$ from other states. (b) A short memory condition for the excited state, i.e., the trajectories of optically excited states diverge away from the initial trajectory within one period. In our case, electron-hole excitations from the ground state as well as from a breather state indeed lead within one period to very different ion trajectories such as separating kink-antikink states. (c) A large amplitude condition, i.e., the oscillating difference in electron energies spans a range larger than $\hbar\omega_B$. This corresponds to a large quantum number n. We are mainly interested in the regime $\hbar\omega\lesssim 2\Delta_0-\hbar\omega_B$ which is dominated by the strongly oscillating intragap states and is separated by more than $\hbar\omega_B$ from other excited states.

The adiabatic eigenfunctions of Eq. (24) and the level occupancy of the breather define an electron wave function $\psi_B(l_{\alpha,s}^{(B)};u_n(t))$, where t is the time parameter on the trajectory and $u_n(t)$ solves Eq. (25). Electron-hole excitations change the level occupancy to $l_{\alpha,s}^{(e)}$ and define excited states $\psi_e(v_{\alpha,s}^{(e)};u_n(t))$; note that with the new occupancy, Eq. (25) with the breather trajectory is not satisfied; the excited state has adiabatic dynamics with different trajectories. Using the current operator [Eq. (A5)] we obtain for its matrix elements

$$\mu_e(t)=\langle\psi_B|J|\psi_e\rangle=-ie\sum_n[t_0+\beta(u_n-u_{n+1})]\times[f_\alpha(n)f_\gamma^*(n+1)-f_\alpha(n+1)f_\gamma^*(n)]/\sqrt{N}. \quad (37)$$

An excitation e is identified by the set $\{\alpha,\gamma\}$ where $\alpha(\gamma)$ is the state that becomes unoccupied (occupied). These states also define an excitation energy $\Delta E_e(t)=\epsilon_\gamma(t)-\epsilon_\alpha(t)$.

The semiclassical formalism shows that most of the transition intensity corresponds to times t for which $\Delta E_e(t)=\hbar\omega$, where ω is the frequency of the electric field. This defines a classically allowed regime $\omega_{\min}<\omega<\omega_{\max}$,

where $\hbar\omega_{\min}=\min_t\{\Delta E_e(t)\}$ and $\hbar\omega_{\max}=\max_t\{\Delta E_e(t)\}$. The short memory condition restricts the excited state to a time range of $T_B=2\pi/\omega_B$; the result for the real part of the conductivity (proportional to the absorption) is then[28]

$$\mathrm{Re}\sigma(\omega)=\sum_e |I_e(\omega)|^2/(2\hbar\omega T_B) , \tag{38}$$

where

$$I_e(\omega)=\int_0^{T_B} dt\, \mu_e(t)\exp\left[-i\omega t+i\int_0^t \Delta E_e(t')dt'/\hbar\right] . \tag{39}$$

In the limit $T_B\to\infty$, where $\mu_e(t)$ and $\Delta E_e(t)$ become time independent, this reduces to the adiabatic result, Eq. (A7).

We proceed to evaluate $\mathrm{Re}\sigma(\omega)$ for the *trans*-$(CH)_x$ model. We use $\lambda=0.34$ as in Sec. III which allows using reasonably short chains while still being in a weak-coupling regime, i.e., gap-to-bandwidth ratio $\simeq 0.4$ is fairly small. For actual *trans*-$(CH)_x$, $\lambda=0.19$ (Ref. 33) with a gap of 1.7 eV and bandwidth of ~ 10 eV. In the weak-coupling regime we expect that the low-energy scale is determined just by the gap $2\Delta_0$. We therefore choose the ratio $\hbar\omega_R/2\Delta_0$ to reproduce the phonon data in *trans*-$(CH)_x$. Choosing $\hbar\omega_R/2\Delta_0=0.110$ yields $E_B(1)/2\Delta_0=0.107$ (Table I); this corresponds to the most strongly coupled Raman-active amplitude phonon[33] in *trans*-$(CH)_x$ at 1460 $\mathrm{cm}^{-1}=0.181$ eV.

Table I shows quantized values of $\bar{\epsilon}$ for the choice $\hbar\omega_R/2\Delta_0=0.11$ and excitation energies; the zero-point energy is $0.11\Delta_0$. The procedure is to use the analytic solution [Eq. (11) with $\eta=1$] as an initial condition for the numerical adiabatic dynamics as in Fig. 4(b). We use an 84-site ring, $\lambda=0.34$, and the three $\bar{\epsilon}$ values of Table I. The nine lowest empty levels (i.e., 43 to 51) for the three cases are shown in Fig. 12. Recall that the nine highest occupied levels are identical to those in Fig. 12 but with opposite sign. The increase in $\bar{\epsilon}$ affects mainly the intragap levels (42 and 43) with pronounced oscillations into the gap region $(-\Delta_0,\Delta_0)$ of the adiabatic limit. The higher levels exhibit level crossing with significant oscillation only in the levels with the same symmetry as the 43rd level.

The eigenvalues of Fig. 12 and the corresponding matrix elements [Eq. (37)] are the input to Eq. (38) for the optical absorption. The formalism assumes independent excited states with no tunneling between them. The crossing levels do not violate this since they have opposite inversion symmetry. The high energy levels are, however, fairy dense and we do not expect that the results for $\hbar\omega\gtrsim 2\Delta_0$ are accurate. Our main interest, however, is in the intragap levels which allow $\hbar\omega<2\Delta_0-\hbar\omega_B$ transitions and for which our formalism is valid.

TABLE I. Quantized values of $\bar{\epsilon}$ for generating breather solutions [Eq. (11) with $\eta=1$]. The excitation energy is E_B [Eqs. (33) and (34)] and the numerically observed frequency is ω_B. The transition energy between the intragap states (42→43 transition) has a mean $\hbar\omega_m$, maximum $\hbar\omega_{\max}$, and minimum $\hbar\omega_{\min}$.

n	$\bar{\epsilon}$	$E_B/2\Delta_0$	$\hbar\omega_B$	$\hbar\omega_m$	$\hbar\omega_{\min}$	$\hbar\omega_{\max}$
0	0.10	0	0.431	3.725	3.442	3.846
1	0.31	0.107	0.425	3.519	2.798	3.846
2	0.55	0.198	0.420	3.356	2.332	3.848

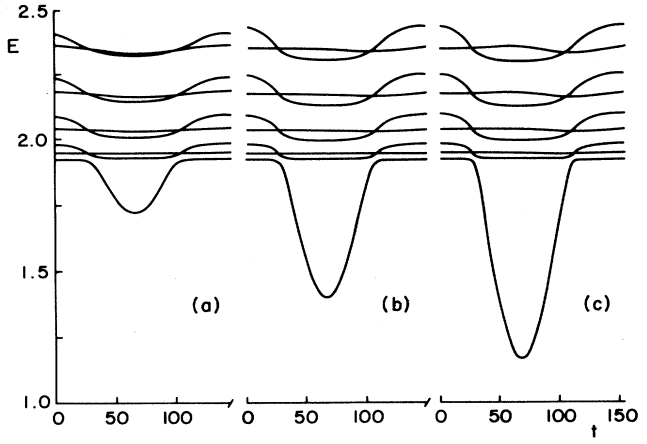

FIG. 12. Lowest occupied electron levels in one period for three breathers with quantized $\bar{\epsilon}$ values (Table I): (a) $n=0$, (b) $n=1$, (c) $n=2$.

Table I also gives the values of $\hbar\omega_m$, $\hbar\omega_{\min}$, and $\hbar\omega_{\max}$ of the intragap transition energies. The large amplitude condition $\omega_{\max}-\omega_{\min}\gg\omega_B$ is marginal for $n=0$ and reasonable for $n=1,2$. Below we also demonstrate a case with the same $\bar{\epsilon}$ values but $\hbar\omega_R$ smaller by a factor 4 so that the large amplitude condition is valid for all the shown cases.

Figure 13 shows the optical absorption of the ground state, i.e., $n=0$ (solid line). The adiabatic gap $2\Delta_0=3.92$

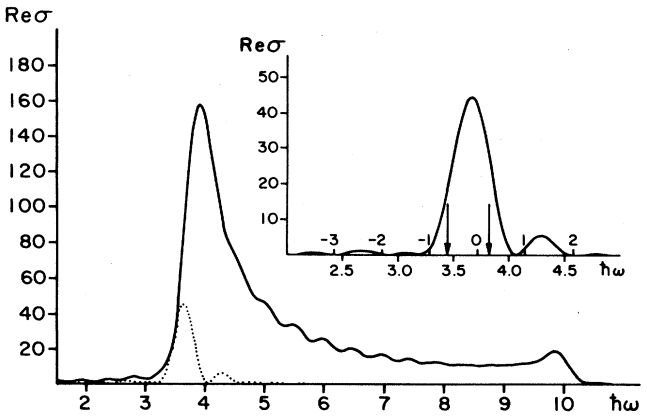

FIG. 13. Optical absorption for the ground state of *trans*-$(CH)_x$ ($n=0$ in Table I) with $N=84$ site ring and $\lambda=0.34$. Solid line is the total absorption, dotted line is the contribution of the intragap (42→43) transition. The inset shows the intragap term in more detail. The arrows show the limits of the classical range $\hbar\omega_{\min}$, $\hbar\omega_{\max}$ while the quantum scale, i.e., the distance from $\hbar\omega_m$ in units of $\hbar\omega_B$ is marked above the axis. The scale for $\hbar\omega$ is set by $t_0=2.5$ [Eq. (23)] or the adiabatic gap of $2\Delta_0=3.92$. $\mathrm{Re}\sigma$ is in units of $e^2/(2Na\hbar)$.

now develops a significant tail at lower frequencies. Most of this tail is due to the intragap states, shown by the dotted line. The oscillations at $\hbar\omega > 2\Delta_0$ are due to the discrete nature of the finite chain eigenvalues. The inset shows this $42 \rightarrow 43$ transition in more detail, indicates the classical regime $(\hbar\omega_{\min}, \hbar\omega_{\max})$, and shows the positions $\hbar\omega_m + n\hbar\omega_B$ with n integer.

Figures 14 and 15 show the results for $\tilde{\epsilon}=0.31$ $(n=1)$ and $\tilde{\epsilon}=0.55$ $(n=2)$, respectively. The increase in $\tilde{\epsilon}$ results in a distinct peak due to the intragap transition. The peak position decreases with $\tilde{\epsilon}$ and is roughly at the mean transition energy $\hbar\omega_m$. Rather strong side bands appear at $\sim\hbar\omega_m \pm 2\hbar\omega_B$ and weaker oscillations with spacing $\hbar\omega_B$ further away from $\hbar\omega_m$.

Figure 16 shows the structure near the gap edge in more detail as well as the absorption *difference* of the excited $n=1,2$ states relative to the ground-state absorption. In particular, we propose that the $n=2$ spectra correspond to the PA data, which show the HE peak at 1.35 eV. We discuss this further in Sec. VII. Figure 16(a) shows the total ground-state absorption as well as the $42 \rightarrow 43$ transition on a logarithmic scale. The arrows show the classical regime beyond which the $42 \rightarrow 43$ absorption decays faster than exponential. A stationary phase calculation shows[28] that indeed in the nonclassical range, e.g., $\omega < \omega_{\min}$,

$$\mathrm{Re}\sigma(\omega) \sim \exp[-(\tfrac{2}{3})(\omega_{\min}-\omega)^{3/2}/d^{1/2}] , \quad (40)$$

where $d=[\partial^2 \Delta E_e(t)/\partial t^2]/2\hbar$ is evaluated at the $\omega_{\min}$ turning point. The total absorption also has contributions from tails of higher excitations and appears roughly as an exponential decay, as do the data on *trans*-$(CH)_x$.[25–27]

To gain insight into these results we define a Fourier decomposition

$$\mu_e(t)\exp\left[i\int_0^t \Delta E_e(t')dt'/\hbar - i\omega_m t\right] = \sum_k g(k)\exp(ik\omega_B t) , \quad (41)$$

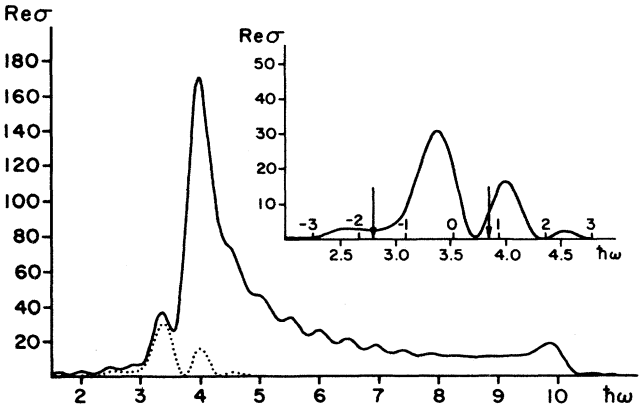

FIG. 14. Same as Fig. 13 for the $n=1$ breather (see Table I).

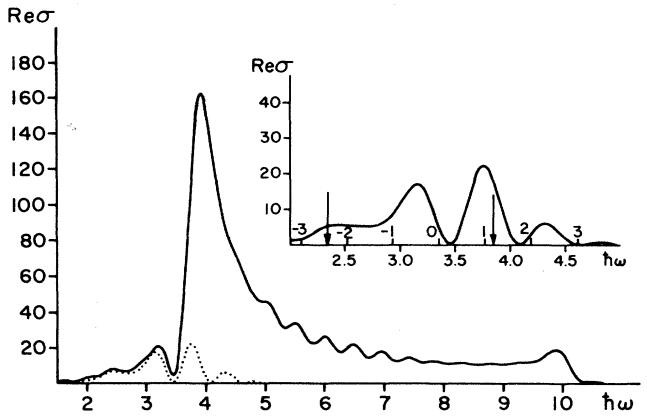

FIG. 15. Same as Fig. 13 for the $n=2$ breather (see Table I).

where $-\infty < k < \infty$ are integers. Equation (39) then becomes

$$I_e(\omega) = i\sum_k g(k)\frac{\exp[-2\pi i(\omega-\omega_m)/\omega_B]-1}{\omega-\omega_m-k\omega_B} . \quad (42)$$

We now define two qualitatively different regimes. The "quantum" regime corresponds to $(\omega_{\max}-\omega_{\min})/\omega_B \gtrsim 1$ but not too large; in this regime only a few k terms are needed in (41) with the largest at $k=0$. A "classical" regime corresponds to $\omega_B \ll \omega_{\max}-\omega_{\min}$ and therefore many terms in expansion (41). A stationary phase calculation[28] shows that (39) is then peaked near $\hbar\omega_{\max}$ and $\hbar\omega_{\min}$.

Figures 13–15 correspond to a quantum regime where the $k=0$ and $k=\pm 2$ terms dominate expansion (41). Note that a dominant single $g(k)$ in (41) leads to zeros of $I_e(\omega)$ at $\omega=\omega_m+k\omega_B$ $(k\neq 0)$ as indeed seen in Figs. 13–15 with $|k| \geq 3$.

To demonstrate the behavior in the classical regime we have used the same input data as above except that the time unit was redefined to be 4 times bigger so that $\hbar\omega_R/2\Delta_0=0.0275$. We use the same $\tilde{\epsilon}$ values, although now they do not correspond to precisely quantized values; $\tilde{\epsilon}=0.1$ is near the $n=2$ value (0.125), $\tilde{\epsilon}=0.31$ is near the $n=5$ value (0.283), and $\tilde{\epsilon}=0.55$ is near the $n=9$ value (0.521). Figures 17–19 show the optical absorption for these cases. The insets demonstrate the classical nature of the intragap transition; as $\tilde{\epsilon}$ increases, the ratio $(\omega_{\max}-\omega_{\min})/\omega_B$ increases and the peaks at $\hbar\omega_{\min}, \hbar\omega_{\max}$ increase. Superimposed on this classical structure are oscillations with spacing $\hbar\omega_B$.

The smaller $\hbar\omega_B$ is also apparent in the $\hbar\omega > 2\Delta_0$ range—the nonclassical tails are smaller and the discrete nature of the spectrum is more pronounced. It is worth pointing out that there is no "natural linewidth" which is introduced by hand in our formulation. The linewidth is due only to ion dynamics and is therefore different in Figs. 13–15 from Figs. 17–19.

In Appendix B we prove a sum rule for $\mathrm{Re}\sigma(\omega)$. We have used this sum rule [Eq. (B4)] to test our numerical matrix elements at any given time on the trajectory with

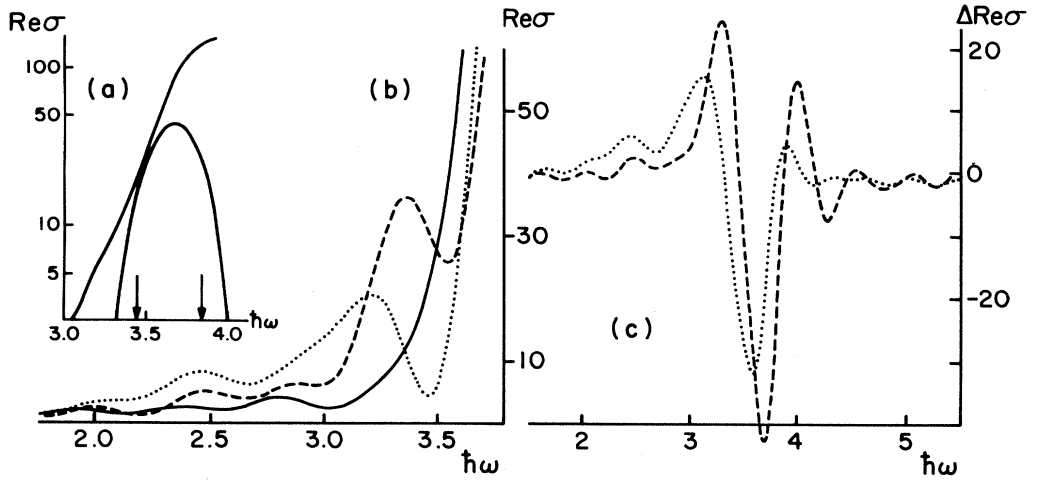

FIG. 16. Absorption near the gap edge for the states of Table I. (a) $n=0$ absorption from intragap states (lower line) and total absorption (upper line) on a logarithmic scale; the arrows show $\hbar\omega_{\min},\hbar\omega_{\max}$. (b) Total optical absorption for $n=0$ (solid line), $n=1$ (dashed line), and $n=2$ (dotted line). (c) Absorption difference of $n=1$ and $n=0$ (dashed line) and that of $n=2$ and $n=0$ (dotted line).

agreement to better than $\frac{1}{2}\%$. We cannot test our final form [Eq. (38)] since we have not attempted to evaluate the right-hand side of Eq. (B4) in a dynamic case. We have, however, evaluated the integrated intensity of the intragap transition Σ_B (which is close to our HE feature intensity) relative to the total intensity Σ_T and found $\Sigma_B/\Sigma_T\simeq 7.1 n_B a$, where $n_B=1/84a$ is the breather density in our simulations; this intensity ratio hardly depends on $\hbar\omega_B/\Delta_0$ or the quantum number n. For comparison, the midgap intensity for a kink Σ_K satisfies[34] $\Sigma_K/\Sigma_T=2.8 m_k\xi$, where n_K is the kink density. Since[2] $\xi=v_F/\Delta_0\cong 7a$ in *trans*-$(CH)_x$ we obtain $\Sigma_K/\Sigma_B=2.8 n_k/n_B$, i.e., similar intensity of a breather HE peak and a kink midgap peak.

To extend these results to the *cis*-$(CH)_x$ and $(AB)_x$ cases, we note that in the quantum regime (Figs. 13–15) the position of the intragap peak is determined mainly by the mean transition energy $\hbar\omega_m$ of the intragap states. We can estimate ω_m to first order in $\tilde{\varepsilon}$ by noting that the local dimerization, Eq. (11), at $x=0$ gives a bound state at energy $\Delta_0(1+\delta)$ when $\delta<0$ and an extended state at Δ_0 when $\delta>0$. The time average then yields

$$\hbar\omega_m(\eta)=2\Delta_0(\eta)\{1-(\tilde{\varepsilon}/\pi)[48\eta/(5+3\eta)]^{1/2}+O(\tilde{\varepsilon}^2)\}\ . \tag{43}$$

In terms of the *trans*-$(CH)_x$ values $\Delta_0(1),\omega_R(1)$ we have $\Delta_0(\eta)=\Delta_0(1)\exp(\eta)$ and $\omega_R(\eta)=\omega_R(1)\sqrt{\eta}$; expressing the quantized $\tilde{\varepsilon}(\eta)$ in terms of $\tilde{\varepsilon}(1)$ finally yields

$$\hbar\omega_m(\eta)=2\Delta_0(1)\{1-\sqrt{6}\tilde{\varepsilon}(1)/\pi+(\eta-1)[1+13\sqrt{6}\tilde{\varepsilon}(1)/16\pi]+O(\tilde{\varepsilon}^2,(\eta-1)^2)\}\ . \tag{44}$$

The effect of increasing the *cis*-polymer parameter $(\eta-1)$ is to increase ω_m, and the rate of increase is higher for

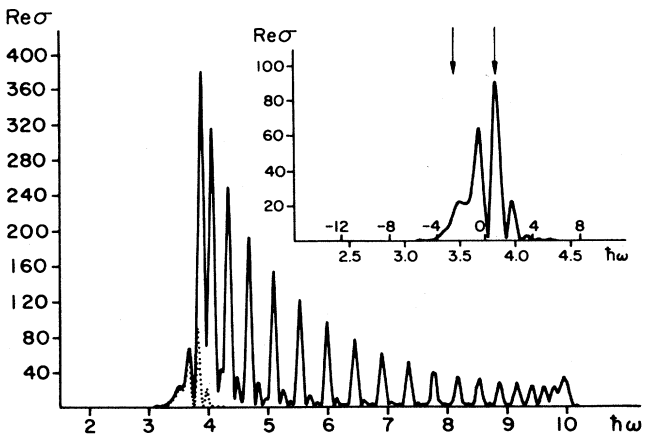

FIG. 17. Same as Fig. 13 for $\tilde{\varepsilon}=0.1$ and $\hbar\omega_R=\hbar\omega_B=0.108$; $\hbar\omega_R$ is 4 times smaller than that of Fig. 13.

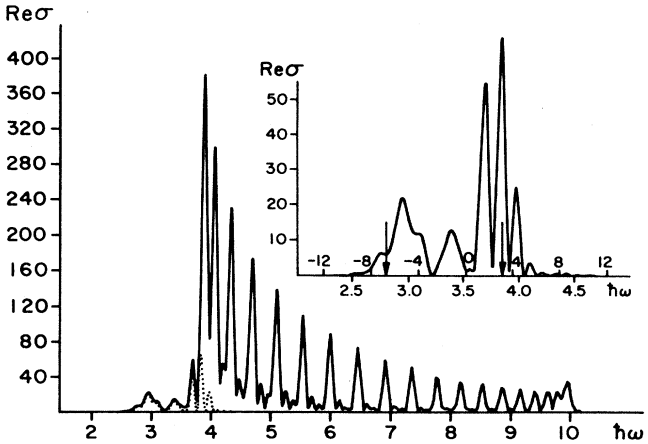

FIG. 18. Same as Fig. 17 for $\tilde{\varepsilon}=0.31$ ($\hbar\omega_B=0.106$).

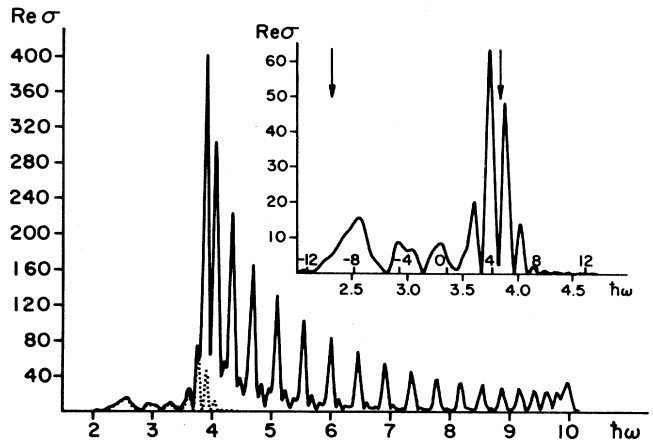

FIG. 19. Same as Fig. 17 for $\bar{\varepsilon}=0.55$ ($\hbar\omega_B=0.105$).

larger $\bar{\varepsilon}$ (or higher n). For the ground state with $\bar{\varepsilon}(1)=0.1$ (Table I), $\hbar\omega_m$ essentially defines the observed gap with

$$[\hbar\omega_m(\eta)-\hbar\omega_m(1)]/2\Delta_0(1)=1.06(\eta-1)\ , \tag{45}$$

while for an $n=2$ breather with $\bar{\varepsilon}(1)=0.55$ (although $\bar{\varepsilon}^2$ terms could be important here)

$$[\hbar\omega_m(\eta)-\hbar\omega_m(1)]/2\Delta_0(1)=1.35(\eta-1)\ . \tag{46}$$

The increased dependence of the HE peak on $(\eta-1)$ was in fact seen experimentally.[19] In a *cis-trans* $(CH)_x$ mixture, the *cis* chains induce a symmetry-beaking term η on the *trans* chains which increases with the *cis*-to-*trans* ratio[35,36] and $(\eta-1)$ is determined by the Raman data.[19] The observed HE peak indeed increases faster than $(\eta-1)$ consistent with (46), although a $\sqrt{\eta-1}$ dependence has been suggested.[19]

The same procedure can be applied to find the effect of an $(AB)_x$ parameter α added to a *trans*-$(CH)_x$-type chain. The result is (recall $\gamma=1-\alpha^2/\Delta_0^2$)

$$\hbar\omega_m(\gamma)=2\Delta_0[1-\sqrt{6}\bar{\varepsilon}(1)(5-4\gamma)/\pi+O(\bar{\varepsilon}^2,(1-\gamma)^4)]\ . \tag{47}$$

Thus the ground-state gap decreases slowly with α while the higher breather states decrease more rapidly with α. Thus the distance of $n=2$ and $n=0$ peaks (i.e., gap minus HE peak) *increase* with α, in contrast with the *cis*-$(CH)_x$ where the distance *decreases* with $(\eta-1)$.

Unlike the *cis*-polymer parameter, the $(AB)_x$ parameter could not yet be experimentally controlled. However, the single studied case[17] of poly(1,6-heptadyine) shows a HE-like feature at ~ 1 eV whose distance from the gap at ~ 2 eV is indeed much larger than the corresponding distance in *trans*-$(CH)_x$.

To conclude this section, we have shown that breathers have specific signatures in optical absorption. Depending on the ratio of breather amplitude to frequency, it can be in a quantum regime with a main absorption peak near $\hbar\omega_m$ (Figs. 13–15), or in a classical regime with main peaks near $\hbar\omega_{\min}$ and $\hbar\omega_{\max}$, the classical turning points.

VI. DISCUSSION

We have shown the existence of breathers in a large class of conjugated polymers by an analytic expansion and by numerical simulations. In general, breathers are found to be dynamically stable, except when an $(AB)_x$-type parameter is too large, i.e., $\alpha/\Delta_0 \gtrsim 0.2$. The long time stability is limited by lattice discreteness in the numerical study and by a possible nonanalytic term[9] even in the continuum theory. The numerical studies, however, show that the breather is a fairly robust object and survives collisions with acoustic phonons. This allows for persistance of breathers in our finite chain simulations. In fact, if the breather is narrow compared with the chain length it exists even for short chains. We have found that an $\bar{\varepsilon}=0.6$ breather (width at 2.5 lattice constants) survives even in a 10-site chain for at least 25 oscillation and is therefore relevant even to finite polyenes. We have also explored[30] the effect of model intrinsic defects in *trans*-$(CH)_x$ and found breathers to be both copiously produced and long lived.

We have used a tight-binding electron-phonon Hamiltonian which neglects direct Coulomb interactions between electrons. These interactions can be included in a Hartree-Fock scheme which shows that the breather solutions are still valid.[37] Exact calculations of excited states are limited to finite chains and to static ions. These calculations have shown[38,39] that the lowest excitation is an A_g state; the lowest one-photon absorption yields a higher-energy B_u state. Two-photon absorption experiments[38] have indeed shown the presence of this A_g state in short polyenes.

Breather excitations also have an A_g symmetry; thus A_g states below the B_u optical gap can bind by either Coulomb correlations in a static lattice, or by nonlinear lattice dynamics in the absence of Coulomb correlations. We expect that the physical A_g states will bind by *both* mechanisms. In short chains only the highly localized breathers are possible, whose high excitation energies are close to those observed in short polyenes. In long chains, however, the breather A_g states form a spectrum from about $2\hbar\omega_R$ (ω_R is practically the Raman frequency) up to $\sim 4\Delta_0/\pi$, above which a breather can decay to a pair of kinks. Since phonon data are consistent with the electron-phonon model,[33,35,36] we expect the low-lying breather states of the long chains to be well described by the electron-phonon Hamiltonian.

We proceed to compare available data with our results. We focus mainly on the HE peak in PA experiments, as seen in *trans*-$(CH)_x$ and related polymers.[12–19] For a gap of $2\Delta_0=1.7$ eV (Ref. 33) the position of the HE peak in *trans*-$(CH)_x$ is 1.35 eV$=0.79\times 2\Delta_0$. Absorption polarized perpendicular to the chains[15] (which eliminates non-HE features) shows that the HE peak is asymmetric with a significant tail down to ~ 1.1 eV$=0.65\times 2\Delta_0$. Our results show that the $n=1$ breather (i.e., an excited phonon) has an induced absorption peak [Fig. 16(c)] at $3.32=0.85\times 2\Delta_0$. The $n=2$ breather has an induced absorption peak at $3.16=0.81\times 2\Delta_0$ and a significant side peak at $2.48=0.63\times 2\Delta_0$. Thus the peak position at the $n=2$ breather is consistent with the HE peak data and its

sideband can account for the pronounced tail at lower frequencies. We note that the $n=2$ breather is the most energetic one allowed by the photogeneration process of electron-hole decaying to kink-antikink plus a breather. Breathers may, however, be photogenerated via other channels which do not involve kink production.

An additional key for the identification of the HE feature is its lifetime, which becomes considerably shorter above 200 K. We note from Table I that the binding energy of an $n=2$ breather relative to two $n=1$ phonons is $0.016\times 2\Delta_0$. For *trans*-$(CH)_x$ this binding is ~ 300 K; the data above 200 K thus indicate the onset of a breather decay into two phonons. Note also that the A_g symmetry of a breather does not allow for a radiative decay, implying a long lifetime at low temperatures.

The HE feature was studied in *trans-cis* $(CH)_x$ mixtures.[19] The signal comes from the *trans* chains which acquire a symmetry-breaking term $\eta-1\neq 0$ from the *cis* environment.[35,36] By analyzing the Raman data[19] it was found that changing the *cis*-trans ratio amounts to changing η in the range $1<\eta<1.04$; this is mostly in the regime allowing direct photogeneration as in Fig. 6(a). The optical gap is expected to change as in Eq. (45) amounting to a 55 meV change at 80% *cis*. The HE peak, however, is shifting more, changing by 95 meV at 80% *cis*. This is consistent with the increased slope of Eq. (46). Data on fully *cis*-$(CH)_x$ have shown a further shift[12,13] of the HE peak to 1.5 eV, though it may be due to remnant *trans* material.

The unique example so far of an $(AB)_x$-type polymer with degenerate minima is poly(1,6-heptadyine). Its PA shows[17] a wide HE-like feature at ~ 1 eV and a shoulder at ~ 0.5 eV. The trend to lower energies is opposite to that of *cis*-$(CH)_x$ and is consistent with Eq. (47). However, the studied sample is amorphous with a second structure probably coexisting.[17] Further studies on better samples should be illuminating.

An alternative explanation of the HE peak is the A_g state stabilized by Coulomb correlations,[12] known to exist in short polyenes.[38,39] As discussed previously, both ion dynamics and Coulomb correlations can contribute to stabilize low-lying A_g states. It would therefore be extremely interesting to follow PA experiments in short polyenes and watch for a HE feature.

The HE feature has also been assigned to neutral solitons which may be photogenerated directly[40] or via a triplet state.[41] Being topological objects, neutral solitons cannot be singly produced on long chains; hence a bound state of neutral solitons was proposed,[14,40,41] although the precise nature of the binding was not specified. Note that a breather can also be viewed as a dynamic bound state of neutral solitons.

The second relevant type of data are the ground-state absorption data. As shown in Fig. 13, the zero-point motion of the ground state leads to a pronounced tail below the adiabatic gap, $\hbar\omega<2\Delta_0$. Figure 16(a) shows the gap-edge region on a logarithmic scale. While the intragap transition (lower line) decays faster than exponential [Eq. (40)], the total absorption appears roughly as an exponential, decaying by a factor of ~ 50 in the energy range 3.1–3.9. Data on *trans*-$(CH)_x$ have shown a similar pronounced absorption tail[25–27] decaying by ~ 100 from 1.7 to 1.3 eV.

It was suggested[26] that this is an Urbach tail due to disorder. While disorder can contribute, we find that most of the tail is accounted for by the nonadiabatic terms. Another contribution to this tail can come from nonadiabatic tunneling into a kink-antikink pair.[42–44] This process is neglected in the short-memory approach which treats the dominant effects in the classical and near-classical regimes.[28] Far from the classical regime, i.e., $\omega\ll\omega_{\min}\lesssim 2\Delta_0$, both Eq. (40) and the kink-antikink process are extremely weak.

We next discuss a few other experiments which can probe the breather states. The A_g symmetry allows breather production by a two-photon process from the ground state. As for short polyenes,[38] this should yield essential information on long polymers. An A_g state can also appear as a resonance in third-order optical susceptibility $\chi^{(3)}$. The limited data[45] on *trans*-$(CH)_x$ indicate a state at 1.8 eV which is above the gap. Photons in the range 0.2–0.5 eV ($\frac{1}{2}$ the breather energies) are needed to excite breather states in a two-photon process.

Inelastic neutron scattering provides an ideal tool for probing breathers, which involve large ion oscillations. The cross section should be comparable to that of scattering from phonons while the energy shifts are higher; e.g., the $n=2$ breather in *trans*-$(CH)_x$ (Table I) has an excitation energy of ~ 0.34 eV. The $n=3$ breather has an excitation energy of $0.45\Delta_0\sim 0.4$ eV (note, however, that our $\tilde{\varepsilon}$ expansion may not be sufficient for this case). We hope that these experiments on *trans*-$(CH)_x$ and related polymers will enhance our understanding of nonlinear dynamics in conjugated polymers.

ACKNOWLEDGMENTS

We thank E. Ehrenfreund, R. N. Friend, Z. G. Soos, and Z. Vardeny for illuminating discussions. S.R.P. and B.H. acknowledge the hospitality of Center for Nonlinear Studies (CNLS) and the Theoretical Division of Los Alamos National Laboratory. B.H. is also thankful for the hospitality of the Laboratory of Atomic and Solid State Physics, Cornell University, Ithaca, New York. This research was supported by a grant from the U.S.-Israel Binational Science Foundation (Jerusalem, Israel). Work of S.R.P. is supported by U.S. Department of Energy (Division of Materials Science, Office of Basic Energy Sciences), under Contract No. W-31-109-Eng-38.

APPENDIX A: CURRENT OPERATORS

The continuum kinetic energy has been replaced by discrete tight-binding terms in Eq. (23), i.e.,

$$H_{\rm el}=-\sum_n [t_0+\beta(u_n-u_{n+1})](C_n^\dagger C_{n+1}+C_{n+1}^\dagger C_n)\ . \tag{A1}$$

The corresponding current operator is now derived. The discrete version of the charge density operator is

$$\rho(n)=eC_n^\dagger C_n\ . \tag{A2}$$

The current operator $J(n)$ is defined on the bond between sites n and $n+1$ so that current conservation is given by

$$-\partial\rho(n)/\partial t = J(n) - J(n-1) . \quad \text{(A3)}$$

Using the Hamiltonian (23) and fermion commutations for C_n we obtain

$$\begin{aligned}(i/e)\partial\rho(n)/\partial t = &[t_0+\beta(u_n-u_{n+1})]C^\dagger_{n+1}C_n \\ &+[t_0+\beta(u_{n-1}-u_n)]C^\dagger_{n-1}C_n \\ &-[t_0+\beta(u_n-u_{n+1})]C^\dagger_n C_{n+1} \\ &-[t_0+\beta(u_{n-1}-u_n)]C^\dagger_n C_{n-1} . \quad \text{(A4)}\end{aligned}$$

The solution of (A3) and (A4) (up to site independent terms) is

$$J(n) = -ie[t_0+\beta(u_n-u_{n+1})](C^\dagger_n C_{n+1} - C^\dagger_{n+1}C_n) . \quad \text{(A5)}$$

Note that the presence of direct electron-electron terms

$$H_{\text{el-el}} = \sum_{n,m} V(n-m)\rho(n)\rho(m) \quad \text{(A6)}$$

in addition to the Hamiltonian (23) does not change the result (A5) since $[\rho(n), H_{\text{el-el}}]=0$.

The conductivity is given in terms of initial state $|\psi_0\rangle$, final states $|\psi_e\rangle$, and their eigenvalues E_0 and E_e, respectively. Standard linear-response theory then yields (at zero temperature)

$$\text{Re}\sigma(q,\omega) = (\pi/\omega)\sum_e |\mu_e(q)|^2\delta(E_e-E_0-\hbar\omega) , \quad \text{(A7)}$$

where

$$\mu_e(q) = \langle\psi_0|J_q|\psi_e\rangle \equiv \left\langle\psi_0\left|N^{-1/2}\sum_{n=1}^{N} J(n)e^{iqn}\right|\psi_e\right\rangle \quad \text{(A8)}$$

and N is the number of sites.

As an example, consider the Hamiltonian (23) in the adiabatic limit, i.e., static u_n. The eigenoperators have the form

$$\hat{f}_\alpha = \sum_n f_\alpha(n)C_n \quad \text{(A9)}$$

which can be inverted to

$$C_n = \sum_\alpha f^*_\alpha(n)\hat{f}_\alpha \quad \text{(A10)}$$

since $f_\alpha(n)$ form a complete set. The many-electron eigenstates are given by $\Pi_\alpha f^+_\alpha|0\rangle$, where $\{\alpha\}$ is a set of occupied states. The operator (A5) can transfer an electron from an occupied state α to an empty state γ with the matrix element

$$\begin{aligned}\mu_{\alpha,\gamma}(q) = -ie\sum_n &[t_0+\beta(u_n-u_{n+1})] \\ &\times[f_\alpha(n)f^*_\gamma(n+1) \\ &-f_\alpha(n+1)f^*_\gamma(n)]e^{iqn}/\sqrt{N} . \quad \text{(A11)}\end{aligned}$$

$\text{Re}\sigma(q,\omega)$ is obtained by substituting (A11) and $E_e-E_0=\epsilon_\gamma-\epsilon_\alpha$ in Eq. (A7), where $\epsilon_\alpha,\epsilon_\gamma$ are the single-particle eigenvalues.

APPENDIX B: CONDUCTIVITY SUM RULE

The commutator $\langle\rho(n),H_{\text{el}}\rangle$ is given by Eq. (A4). It is straightforward to evaluate the nested commutator and obtain the operator identity

$$\sum_{n,m}[\rho(m),[\rho(n),H_{\text{el}}]]e^{iq(n-m)} = 4e^2\sin^2(q/2)H_{\text{el}} . \quad \text{(B1)}$$

This commutation can also be calculated from Eq. (A3) from which $i[\rho(n),H_{\text{el}}]=j(n)-j(n-1)$ is used for the inner commutator. The outer commutator is evaluated by substituting a complete intermediate set and using

$$\langle\psi_\alpha|\rho(n)|\psi_\beta\rangle = -i\frac{\langle\psi_\alpha|[j(n)-j(n-1)]|\psi_B\rangle}{E_\beta-E_\alpha} . \quad \text{(B2)}$$

Equating both results of the double commutator and taking an expectation value in state ψ_α yields

$$\begin{aligned}2N\sin^2(q/2)\sum_\beta &\frac{|\langle\psi_\alpha|J_q|\psi_\beta\rangle|^2}{E_\beta-E_\alpha} \\ &= -e^2\sin^2(q/2)\langle\psi_\alpha|H_{\text{el}}|\psi_\beta\rangle . \quad \text{(B3)}\end{aligned}$$

Note that we must keep $q\neq0$ up to this point. Canceling $\sin^2(q/2)$ and using Eq. (A8) yields the conductivity sum rule (assuming $E_e>E_0$)

$$\int_0^\infty d\omega\,\text{Re}\sigma(q,\omega) = -(\pi/2N)e^2\langle\psi_0|H_{\text{el}}|\psi_0\rangle . \quad \text{(B4)}$$

Note that the presence of direct Coulomb interactions [Eq. (A6)] does not affect this sum rule since $[\rho(n), H_{\text{el-el}}]=0$. The form (A5) of the current operator which satisfies (A3) is essential in deriving the sum rule.

In the continuum limit $t_0\to\infty$, $a\to0$, and the effects of dimerization or that of Coulomb terms (A6) can be neglected when evaluating $\langle H_{\text{el}}\rangle$; the leading term is the tight-binding spectrum $-2t_0\cos(ka)$ with occupied states in the wave-vector range $|k|<\pi/a$. Equation (B4) then reduces to

$$\int_0^\infty d\omega\,\text{Re}\sigma(q,\omega) = e^2v_F , \quad \text{(B5)}$$

where $v_F=2t_0a$ is the Fermi velocity. Equation (B5) was also derived directly from the continuum model.[33]

[1]For recent reviews, see Synth. Met. **17**, 27 (1987).

[2]W. P. Su, J. R. Schrieffer, and A. J. Heeger, Phys. Rev. Lett. **42**, 1698 (1979); Phys. Rev. B **22**, 2099 (1980); **28**, 1138(E) (1983).

[3]S. A. Brazovskii, Pis'ma Zh. Eksp. Teor. Fiz. **28**, 656 (1978) [JETP Lett. **28**, 606 (1978)].

[4]H. Takayama, Y. R. Lin-Liu, and K. Maki, Phys. Rev. B **21**, 2388 (1980).

[5]B. Horovitz, Phys. Rev. B **22**, 1101 (1980); **35**, 734 (1987).
[6]A. C. Scott, F. Y. F. Chu, and D. W. McLaughlin, Proc. IEEE **61**, 1443 (1973).
[7]C. A. Wingate, SIAM (Soc. Ind. Appl. Math.) J. Appl. Math. **43**, 120 (1983).
[8]D. K. Campbell and J. W. Negele (unpublished).
[9]H. Segur and M. D. Kruskal, Phys. Rev. Lett. **58**, 747 (1986); Y. S. Kivshar and B. A. Malomed, *ibid.* **60**, 164 (1988).
[10]W. P. Su and J. R. Schrieffer, Proc. Natl. Acad. Sci. USA **77**, 5626 (1980).
[11]R. Ball, W. P. Su, and J. R. Schriffer, J. Phys. (Paris) Colloq. **44**, C3-429 (1983).
[12]For a review, see J. Orenstein, in *Handbook of Conducting Polymers,* edited by T. A. Skotheim (Dekker, New York, 1986), p. 1297.
[13]J. Orenstein and G. L. Baker, Phys. Rev. Lett. **49**, 1043 (1980).
[14]Z. Vardeny, J. Tanaka, H. Fujimoto, and M. Tanaka, Solid State Commun. **50**, 937 (1984).
[15]P. D. Townsend and R. H. Friend, J. Phys. C **20**, 4221 (1987).
[16]J. Orenstein, G. L. Baker, and Z. Vardeny, J. Phys. (Paris) Colloq. **44**, C3-407 (1983).
[17]R. Zemach, Z. Vardeny, O. Brafman, E. Ehrenfreund, A. J. Epstein, R. J. Weagley, and W. H. Gibson, Mol. Cryst. Liq. Cryst. **118**, 423 (1985).
[18]E. Ehrenfreund, Z. Vardeny, O. Brafman, R. Weagley, and A. J. Epstein, Phys. Rev. Lett. **57**, 2081 (1986).
[19]Z. Vardeny, E. Ehrenfreund, and O. Brafman, Synth. Met. **17**, 349 (1987).
[20]A. R. Bishop, D. K. Campbell, P. S. Lomdahl, B. Horovitz, and S. R. Phillpot, Phys. Rev. Lett. **52**, 671 (1984); Synth. Met. **9**, 223 (1984).
[21]S. R. Phillpot, A. R. Bishop, and B. Horovitz, J. Phys. C **20**, L485 (1987).
[22]S. A. Brazovskii and N. N. Kirova, Sov. Sci. Rev. A **5**, 99 (1984).
[23]M. J. Rice and E. J. Mele, Phys. Rev. Lett. **49**, 1455 (1982).
[24]B. Horovitz and B. Schaub, Phys. Rev. Lett. **50**, 1942 (1983).
[25]C. R. Fincher, Jr., M. Ozaki, M. Tanaka, D. Peebles, L. Lauchlan, A. J. Heeger, and A. G. MacDiarmid, Phys. Rev. B **20**, 1589 (1979).
[26]B. R. Weinberger, C. B. Roxlo, S. Estemad, G. L. Baker, and J. Orenstein, Phys. Rev. Lett. **53**, 86 (1984).
[27]G. Leising, H. Kahlert, and O. Leitner, in *Electronic Properties of Polymers and Related Compounds,* Vol. 63 of *Springer Series in Solid State Sciences,* edited by H. Kuzmány, M. Mehring, and S. Roth (Springer, Berlin, 1985), p. 56.
[28]B. Horovitz, A. R. Bishop, and S. R. Phillpot, Phys. Rev. Lett. **60**, 2210 (1988); Phys. Rev. A (to be published).
[29]B. Horovitz and J. A. Krumhansl, Phys. Rev. B **29**, 2109 (1984).
[30]S. R. Phillpot, D. Baeriswyl, A. R. Bishop, and P. S. Lomdahl, Phys. Rev. B **35**, 7533 (1988). Relevant details are in Appendix C.
[31]D. K. Campbell and A. R. Bishop, Phys. Rev. B **24**, 4859 (1981).
[32]R. F. Dashen, B. Hasslacher, and A. Neveu, Phys. Rev. D **11**, 3424 (1975).
[33]E. Ehrenfreund, Z. Vardeny, O. Brafman, and B. Horovitz, Phys. Rev. B **36**, 1535 (1987).
[34]B. Horovitz, Solid State Commun. **41**, 593 (1982).
[35]Z. Vardeny, E. Ehrenfreund, O. Brafman, and B. Horovitz, Phys. Rev. Lett. **54**, 75 (1985).
[36]B. Horovitz, Z. Vardeny, E. Ehrenfreund, and O. Brafman, J. Phys. C **19**, 7291 (1986).
[37]M. Sasai and H. Fukutome, Prog. Theor. Phys. **79**, 61 (1988).
[38]B. Hudson, B. E. Kohler, and K. Schulten, in *Excited States,* edited by E. C. Lim (Academic, New York, 1982), Vol. 6, p. 1; B. Hudson and B. Kohler, Synth. Met. **9**, 241 (1984).
[39]Z. G. Soos and L. R. Ducasse, J. Chem. Phys. **78**, 4092 (1983).
[40]S. Kivelson and W. K. Wu, Phys. Rev. B **34**, 5423 (1986).
[41]W. P. Su, Phys. Rev. B **36**, 6040 (1987).
[42]J. P. Sethna and S. Kivelson, Phys. Rev. B **26**, 3513 (1982).
[43]Zhao-bin Su and Lu Yu, Phys. Rev. B **27**, 5199 (1983).
[44]A. Auerbach and S. Kivelson, Phys. Rev. B **33**, 8171 (1986).
[45]F. Kajzar, S. Etemad, G. L. Baker, and J. Messier, Synth. Met. **17**, 563 (1987).